The Dissertation Committee for Stephen Alexander Herrmann certifies that this is the approved version of the following dissertation:

Non-invasive optoacoustic monitoring of neonatal cerebral venous oxygen saturation

Committee:

Rinat Esenaliev, PhD, Supervisor

Donald Prough, MD, Co-Supervisor

Giulio Taglialatela, PhD

Maria Micci, PhD

Claudia Robertson, MD

Dean, Graduate School

Non-invasive optoacoustic monitoring of neonatal cerebral venous oxygen saturation

by

Stephen Alexander Herrmann, MS, MD

Dissertation

Presented to the Faculty of the Graduate School of

The University of Texas Medical Branch

in Partial Fulfillment

of the Requirements

for the Degree of

Doctor of Philosophy

The University of Texas Medical Branch
June, 2018

Dedication

To my beautiful and loving wife, Amanda, and our wonderful two boys, Henry and

Patrick, who provide support and light to my life.

Acknowledgements

Rinat Esenaliev

Irene Petrov

Yuri Petrov

Donald Prough

Rafael Fonseca

Joan Richardson

Non-invasive optoacoustic monitoring of neonatal cerebral venous oxygen saturation

Publication No._____

Stephen Alexander Herrmann, PhD

The University of Texas Medical Branch, 2018

Supervisor: Rinat Esenaliev, PhD

Peripartum asphyxia is a common cause of cerebral hypoxia and when severe can lead to neuronal injury and hypoxic-ischemic encephalopathy (HIE) in the newborn. HIE has been reported up to 3/1000 live births with a high mortality of up to 50% and 25% of survivors developing permanent neurological disabilities. Cerebral hypoxia in neonates is a diagnostic challenge due to a combination of poor correlation between hypoxia severity and physical exam findings, as well as a lack of methodology to quickly and accurately measure cerebral venous oxygen saturation. While diagnosis of neonatal cerebral hypoxia is limited, treatment with cerebral hypothermia has shown to decrease both mortality and long-term neurodevelopmental disabilities in neonates with moderate to severe cerebral hypoxia. Clinicians are still in need of timely and accurate tests to diagnose cerebral hypoxia prior to treatment. Invasive internal jugular (IJ) catheters can provide an assessment of cerebral hypoxia with poor clinical outcomes seen once saturation is below 50%, but this method of assessment is not practical for routine screening use in a neonate due to risks and procedure complications. A non-invasive measurement of cerebral venous oxygen saturation could diagnose cerebral hypoxia earlier and help stratify neonates at risk to further improve clinical outcomes. Our project objective is to evaluate a laser

optoacoustic device for non-invasive monitoring of cerebral venous oxygen saturation through the open anterior/posterior fontanelles in neonates. Sheep models have shown this device can accurately measure cerebral venous oxygen saturation. We initially evaluated our laser optoacoustic system using plastisol phantoms of the neonate superior sagittal sinus, and then obtained measurements from clinically stable neonates in the UTMB neonatal intensive care unit. Analysis of these neonates provided initial data on the range of cerebral venous oxygen saturation levels in clinically stable neonates. The ultimate goal of this work is to identify a device that can quickly and accurately diagnose neonates at risk for cerebral hypoxia and in turn improve mortality and neurological disabilities in these at-risk patients.

TABLE OF CONTENTS

List of Tables

List of Figures

List of Abbreviations

Arb.Un.   Arbitrary Units

CT   Computed Tomography

Fi02   Fraction inspired 02

Hb   Hemoglobin

HIE   Hypoxic-Ischemic Encephalopathy

IJ   Internal Jugular

LDS   Laser Diode System

MRI   Magnetic Resonance Imaging

MRS   Magnetic Resonance Spectroscopy

MRV   Magnetic Resonance Venography

NIRS   Near Infrared Spectroscopy

OPO   Optical Parametric Oscillator

PVC-P   Ployvinylchloride Plastisol

PVDF   Polyvindylidene Flouride

SjO_2 Jugular venous oxyhemoglobin saturation

SSS   Superior Sagittal Sinus

US   Ultrasound

Chapter 1 INTRODUCTION

Cerebral Hypoxia in Neonates

Cerebral hypoxia is a lack of oxygen supply to the brain and occurs due to many etiologies in adults, such as traumatic brain injury or stroke, but in neonates commonly manifests due to peripartum asphyxia in which hypoxia leads to impaired oxidative metabolism and subsequent excitotoxicity. When cerebral hypoxia is severe the term more commonly used is hypoxic ischemic encephalopathy (HIE), with an incidence of 3/1000 live births [1–3] in developed countries and estimated much higher in undeveloped countries [4,5]. Globally, asphyxia has been implemented in millions of neonatal deaths [6]. Approximately 20-50% of newborns with HIE die within the first month of life, and 25% of survivors develop permanent neurological deficits [1]. Lack of perfusion during this period is a major contributor to both neonatal morbidity and mortality, causing multiple long term neurological disabilities including mental retardation, motor dysfunction and epilepsy [1,3,7,8]. Unfortunately, there has been minimal improvement in diagnosis of cerebral hypoxia in neonates and infants because clinical exam is the current primary method of evaluation and diagnostic tests are not available.

Mechanisms of cerebral hypoxia injury stem from prior rat models [1,9] in which carotid artery ligation or low oxygen inhalation led to cerebral hypoxia causing impaired oxidative dysfunction and subsequent anaerobic metabolism causing lactic acid accumulation. Additionally it is thought glutamate imbalance and mitochondrial dysfunction contribute to eventual reactive oxygen species formation, cell death apoptosis and necrosis [2,10]. Interestingly, piglet, rat, and neonatal modes [11,12] suggest that injury from cerebral hypoxia occurs in two phases, with an immediate neuronal injury in severe hypoxia followed by a latent period of several hours (6-24 hrs) in which a delayed energy failure occurs [2,13] leading to further injury and neonatal encephalopathy. This

delayed phased has been supported by accumulation of metabolites related to neuronal death when evaluated with magnetic resonance spectroscopy (MRS). This second phase of injury is thought to be a major contributor to neonatal encephalopathy and a majority of the cell death [13]. Additionally decreased cerebral blood flow is believed to occur in conjunction with severe hypoxia due to impaired cardiac output with shunting of blood from the anterior cerebral circulation to posterior cerebral circulation in order to maintain adequate oxygen supply to the brainstem, preserving respiratory function with injury limited to the peripheral cortex and watershed territories [5].

The clinical manifestations of cerebral hypoxia are described as neonatal encephalopathy, and include multiple exam findings such as seizures, altered consciousness, respiratory depression, poor feeding, abnormal muscle tone, and others [2,5,10]. While these clinical findings are apparent with severe HIE, evaluation for hypoxia becomes more difficult with mild and moderate HIE [3]. Longitudinal studies that followed neonates with severe hypoxia demonstrated profound mental and physical development delays such as in cerebral palsy, with much more variable outcomes in mild/moderate hypoxia cases. The Sarnat staging classification system for HIE has been developed to categorize infants into mild/moderate/severe HIE based on physical exam findings and duration of symptoms, although there is variable correlation with outcome [3]. When hypoxia is severe, multiple clinical conditions and diagnostic tools can suggest prognosis, including abnormal fetal heart tones, metabolic acidosis, delayed onset spontaneous breathing, arterial cord blood sampling, abnormal APGAR scores, multiple organ failure, or known hypoxic event (i.e. uterine rupture, nuchal cord, placentae abruption) [3,8,14].

Fortunately, the recent development of hypothermia treatment protocols [2,13,15–17] for HIE have shown improved outcomes both in morbidity and mortality, although there is debate with timing of treatment and variable outcomes with less severe hypoxia. As a delayed neuronal injury is thought to occur hours after the initial hypoxic insult, a suggested treatment window of when neonates should receive therapy to prevent further

injury is under evaluation [2,13]. The combination of difficulty with clinical examination, variable outcomes, therapeutic window and recent development of treatment emphasize the need for a diagnostic test that can provide quick and accurate assessment of cerebral hypoxia to stratify patients and guide physicians in clinical management.

Treatment of Cerebral Hypoxia in Neonates

Initial treatment for suspected HIE typically has traditionally involved supportive care, and consists of maintaining respiratory oxygenation, blood pressure, fluid/nutrition status, and use of antiepileptics [5] if seizures occur. The recent identification of hypothermia as a means to reduce hypoxic injury in cases of HIE has been explored with both whole body and selective head cooling [18]. Neonates are cooled to 33.5˚C-35˚C, with multiple studies demonstrating a statistically significant improvement in both morbidity and mortality in neonates diagnosed with moderate-severe HIE to 18 months of age [13]. Additional studies were followed up at 22 month and 7-8 years, and demonstrated continued improved outcomes in neonates who had received hypothermia [5,15,19]. Long term developmental deficits are seen even in neonates who did not have significant disabilities initially, as there appears to be subtle deficits seen in cognitive skills such as reading, writing and memory as well as deficits in fine/gross motor skills and increased rates of attention deficit-hyperactivity disorder in these patients [15,19]. Hypothermia is considered to be safe without any increased neurodevelopmental deficits when compared to supportive care, and is considered standard of care for moderate/severe HIE [15,18]. Hypothermia does cause complications such as arrhythmias and coagulopathy, but these conditions are more commonly noted at temperatures that are not used for treatment of HIE [20].

Although these studies show hypothermia can improve clinical outcomes in neonatal HIE, there is uncertainty on when to implement hypothermia and the duration of

treatment. Additionally, there has not been a notable improvement in outcomes for mild/moderate HIE [13]. Some initial studies show that early initiation of hypothermia treatment had improved outcomes [15] when compared to later implementation [18]. Specifically, treatment before 3 hours of age demonstrated improved motor outcomes in neonates with moderate-severe hypoxia compared to treatment after 3 hours, underscoring the need for a diagnostic test for the diagnosis of HIE that can be rapidly administered and interpreted [18].

While the underlying goal of hypothermia therapy is to reduce neuronal tissue injury, the mechanism of hypothermia treatment success is not well understood. Hypothermia has long been used as a neuroprotective strategy after cardiac arrest [20]. The proposed physiology is that hypothermia leads to reduced energy consumption, leading to decreased lactic acid and glutamate accumulation and a subsequent decrease in inflammation and programed cell death [2,13,20]. Studies in piglets treated with hypothermia demonstrated a decrease in the number of apoptotic cells [12,21]. Additionally recent evaluation of neonates with HIE treated with hypothermia demonstrated improved neurological outcomes in those which had preserved mean arterial pressure [22]. Both head and whole-body cooling studies demonstrate hypothermia can improve both morbidity and mortality. More studies are needed to evaluate when and how long treatment should be implemented, which neonates are most at risk and evaluation of management with traditional conservative therapies. Clinicians are in need of a rapid and accurate diagnostic test that could both screen and stratify neonates for cerebral hypoxia.

Invasive Monitoring of Cerebral Hypoxia

In the adult patient, monitoring of cerebral hypoxia utilizes invasive catheterization of the internal jugular (IJ) vein to measure jugular venous oxyhemoglobin saturation (SjO_2). The internal jugular veins receive blood from the entire brain as a common drain

of the sigmoid sinuses. The internal jugular veins vary in size, with the right typically larger and thus more commonly accessed [22, 25]. There is debate whether this would affect unilateral brain injury evaluation [26]. Currently SjO_2 is used in multiple clinical settings, including traumatic brain injury (TBI), stroke, and during cardiovascular surgery as a marker for cerebral hypoxia [23]. Previous studies have shown poor outcomes in adults when prolonged IJ venous oxygen saturation is below 50%, with upper limits of normal range at 75% [23–25]. The cerebral hemodynamics in the neonate are not well understood, and are likely dynamic and complex due to changes from in-utero life and immediate postnatal changes. There is limited data on the normal range of venous oxygen saturation levels in neonates, with data from near-infrared Spectroscopy (NIRS) studies showing variability within the first few weeks of postnatal life [26] and with elevated tissue saturation levels in neonates with hypoxia who had worse later outcomes [27].

As mentioned previously, SjO_2 is obtained in the adult by inserting a fiber optic catheter into the IJ vein, and is estimated based on the differences of absorption coefficient of oxygenated hemoglobin. Different wavelengths can be used to calculate SjO_2. Typically one fiber directs the light and another fiber absorbs the reflected light at different wavelengths to provide the oxygen saturation measurements [28].

Unfortunately, this method estimates the SjO_2 from IJ venous oxygen saturation, which is representative of blood returning from the entire brain. Measurements may be artefactual with injury in neonates due to suggested autoregulation that occurs during hypoxia in which blood is shunted from cortical structures to the brainstem in order to preserve respiratory status [5]. The superior sagittal sinus (SSS) (Figure 1) is a major blood vessel that drains the cortical structures. Measurements from this structure could provide an earlier and more accurate assessment of neonatal cerebral hypoxia, as blood from the cortex and not the brainstem drains into this important vein, and may provide a more accurate representation of cerebral oxygen saturation. In support of this, prior piglet studies have shown differences between direct measurements from IJ vein and SSS [29]. As the

methodology stands, SjO_2 acquisition requires an invasive procedure, which holds inherent risks including accidental internal carotid puncture, venous thrombosis, subcutaneous hematoma, line infection/sepsis and others [23,30]. While these risks are considered low in adults due to the large vein size and the current use of ultrasound guidance, the procedure would not be acceptable as a screening tool in neonates due to these multiple risk factors, enforcing the need for safe alternative methods for cerebral venous oxygen saturation.

An additional, less invasive test to evaluate for fetal distress during labor includes fetal scalp blood pH analysis. The scalp can commonly be accessed through the vaginal canal during labor and scalp blood can be analyzed to evaluate for metabolic acidosis, a sign of hypoxia. This could be pursued if there was concern for fetal distress such as abnormal fetal heart tones on electronic fetal heart rate monitoring. Unfortunately there was no significant correlation of outcomes with scalp blood pH and the procedure has a high sampling failure rate [31].
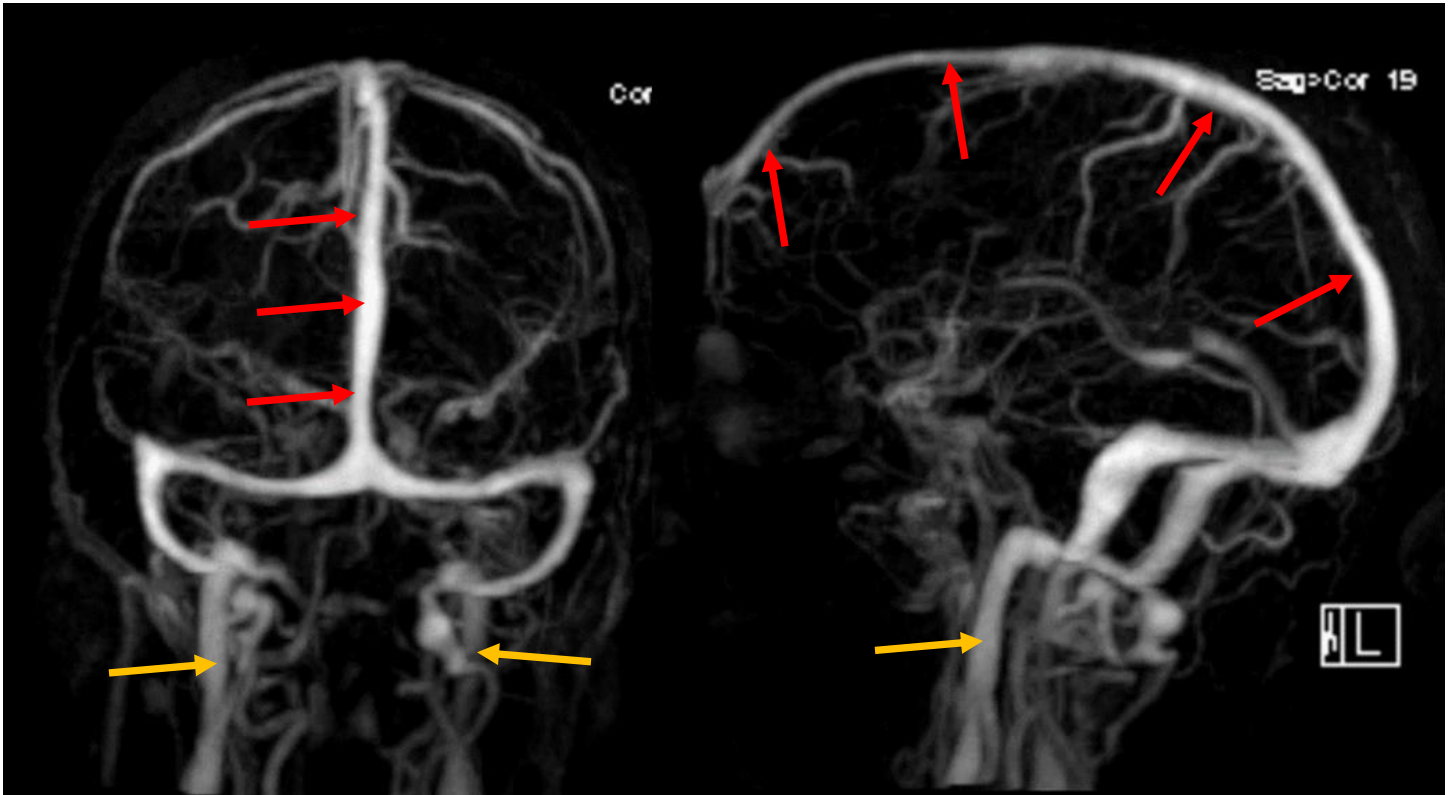
Figure 1: Magnetic resonance venography coronal (A) and sagittal (B) images demonstrating the superior sagittal sinus (red arrow) which eventually drains to the internal jugular veins (yellow arrows).

Non-Invasive Monitoring of Cerebral Hypoxia

Due to risks with invasive catheter placement and the need for rapid neonatal evaluation of cerebral hypoxia, there have been multiple attempts to provide a quick non-invasive diagnostic and prognostic tests such as near-infrared spectroscopy (NIRS), electroencephalogram (EEG), magnetic resonance imaging (MRI), magnetic resonance

spectroscopy (MRS) and cerebral ultrasound (US), but with variable outcomes [32]. The use of EEG evaluates the electrical activity of the overlying cerebral cortex that can be used both safely and quickly. Poor outcomes are seen in HIE when seizures [33] are involved but more studies are needed to evaluate subtle EEG changes when no seizures have occurred. MRI can provide exquisite detail of brain anatomy with diffusion weighted imaging (DWI) delineating areas of early ischemic changes accurately, but unfortunately they are time extensive, expensive and neonates would need sedation, excluding its use as a quick screening tool. MRS can evaluate metabolites in the brain which are used as markers for ischemia, such as lactate and choline, but encounters similar issues that occur with MRI. Cerebral ultrasound is quick and cost-effective, and typically show structural injury changes from extensive hypoxia. Unfortunately these examinations commonly identify changes of ischemic insult that have occurred after the delayed neuronal injury [5] outside the proposed therapeutic window, limiting their roles in the detection of neonatal hypoxia.

Currently electronic fetal monitoring (EFM) is one of the most common ways used to estimate for peripartum fetal distress, and involves monitoring fetal heart rate as well as maternal uterine contraction. Alteration of fetal heart rate such as tachycardia or bradycardia can be seen with fetal distress and are thought to occur from hypoxia and HIE, but a large false positive rate has also been identified with this modality [34]. While EFM is thought to decrease neonatal morbidity/mortality by allowing for early intervention such as a cesarean section, there has been debate on the actual improvement of neonatal outcome [35] and could potentially be a source of unnecessary increased surgical intervention [36].

NIRS is a noninvasive method to monitor regional cerebral oxygenation by measuring light returning from strongly scattering tissues. NIRS transmits light via a fiber optic which is received by an optical detector after passing through tissues of varying density (Figure 2). The differences in the two wavelengths are used to calculate oxygenation of the cerebral tissues [37,38]. Unfortunately this technology cannot evaluate

8

oxygen saturation from individual veins as it assesses superficial regional brain tissue oxygenation (mixture of arterial/capillary/venous blood) [39,40]. This regional measurement may limit the ability of NIRS to identify cerebral hypoxia due to proposed cerebral autoregulation during brain ischemia in which vasodilation would increase arterial oxygen saturation altering the measurements seen with NIRS [26]. Direct venous oxygen saturation measurements from a major cortical draining vessel such as the SSS could provide a more accurate assessment of venous oxygen saturation status [41] rather than a measurement of mixed vasculature oxygenation. Additionally, study-to-study variability is another important limitation of this technology [42–44].
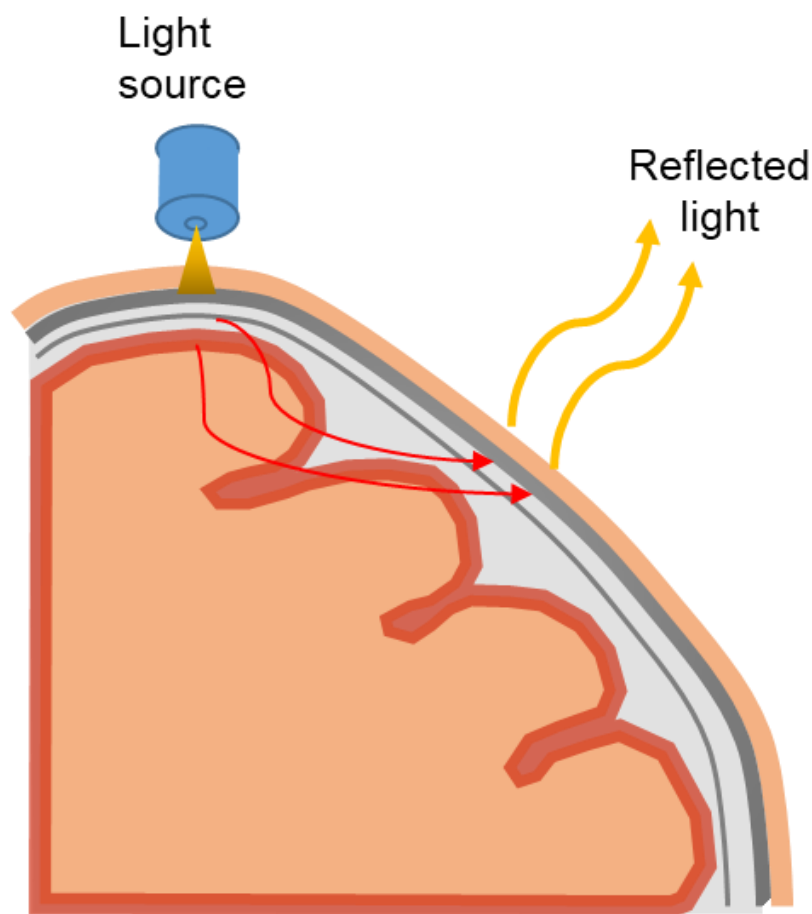
Figure 2: Illustration of NIRS signal acquisition from cerebral and overlying tissues.

We have designed a novel optoacoustic laser device which uses optoacoustic (ultrasound) waves generated by pulsed light to target an individual vessel to measure cerebral venous oxygen saturation. The optoacoustic technology combines optical contrast with ultrasound resolution. Using this technology we can target a large cerebral draining vein such as the superior sagittal sinus (SSS) in order to measure venous oxygen saturation, rather than a mixture of signals from vessels and parenchyma as seen in NIRS. We propose that our novel non-invasive optoacoustic device can target the neonatal SSS and measure SSS venous oxygen saturation. First, we will evaluate our device in a neonatal SSS plastisol phantom. Subsequently, we will evaluate optoacoustic signal acquisition and SSS oxygen saturation measurements in a group of healthy neonates. This preliminary study will provide crucial initial information on the capability of our device to obtain signal in a variety of neonates and the range of cerebral oxygen venous saturation in clinically stable neonates.

Chapter 2 PRINCIPLES OF OPTOACOUSTICS

Optoacoustic Background

The basis of optoacoustics is that absorption of light in a media will lead to an increase in temperatures inducing thermal expansion with subsequent pressure wave production that can be detected with an ultrasound probe (Figure 3). The combination of optical generation of optoacoustic waves with time-resolved detection of the waves allows for oxygen saturation measurements directly from vessels such as the SSS.

Figure 3: Optoacoustic pressure wave generation by light pulses.

The thermal expansion pressure formation $P(z)$ after administration and absorption of light energy in a media can be calculated by following equation:

$$P = \rho_o c_s^2 \beta \Delta T \qquad (1)$$

in which ρ_o (kg/cm^3) is the medium density, c_s (cm/s) is the speed of sound, β (1/°C) is the thermal expansion coefficient, and ΔT (K) is the temperature increase within the medium. The temperature rise is related to the laser fluence (F):

$$\Delta T = \mu_a F / \rho_o c_p \qquad (2)$$

in which C_p (J/g°C) is heat capacity, $F(z)$ (J/cm^2) is laser fluence, and μ_a (cm^{-1}) is the absorption coefficient of the medium irradiated. When these equations are combined we obtain:

$$P(z) = (\beta c_s^2 / C_p) \, \mu_a F(z) = \Gamma \mu_a F(z) \qquad (3)$$

in which the Grüneisen parameter $\Gamma = \beta c_s^2 / C_p$. Per Beer-Lambert law, transmittance decreases exponentially in an absorbing medium:

$$F(z) = F_0 e^{-\mu_a z} \qquad (4)$$

The absorption within the media can be combined with the prior equation for the following:

$$P(z) = \Gamma \mu_a F(z) = \Gamma \mu_a \, F_0 e^{-\mu_a z} \qquad (5)$$

These equations demonstrate how the pressure wave amplitude received by the ultrasound probe is proportional to laser fluence, absorption coefficient of media and Gruneisen parameter [45]. As z and t are related as: $z = c_s t$, then the temporal profile $P(t)$ of the signal obtained is proportional the attenuation coefficient of the media as well as speed of sound:

$$P(t) = \Gamma \mu_a F_0 e^{-\mu_a c_s t} \tag{6}$$

With these equations we can then measure the depth of the blood vessel of interest. As the pressure depends linearly on the absorption coefficient we can evaluate the varying absorption coefficients between both oxygenated and deoxygenated hemoglobin. When light interacts with a strongly scattering medium there are three major types of interactions: absorption, scattering and effective attenuation. They are characterized by absorption (μ_a), scattering (μ_s) and effective attenuation (μ_{eff}) coefficients [45,46]. The effective attenuation in scattering media is described as:

$$\mu_{eff} = \sqrt{3\mu_a \left(\mu_a + \mu_s(1-g)\right)} \tag{7}$$

The anisotropy factor (g) defines whether light is scattered forward, backward or in other directions [47]. In the near infrared spectral range (600-1300 nm), which is the range of our pulsed lasers, there is decreased scattering and absorption coefficients of tissues that allows for deeper penetration of light. From the previous equations we can incorporate the effective attenuation coefficient as follows:

$$P(t) = \Gamma \cdot \mu_a F_0 e^{(-\mu_{eff} c_s t)} \tag{8}$$

With this equation there is a direct relationship of the signal temporal profile with the attenuation coefficient of oxygenated hemoglobin and speed of sound. As the

12

absorption coefficient of hemoglobin depends on its oxygenation, we can predict the oxygen saturation based on different pressure amplitude generation. We can predict hemoglobin oxygen saturation by using the coefficients of a linear fit ratio to the interpolated data of hemoglobin oxygen saturation levels. Since the amplitude of optoacoustic signal generated is linearly proportional to the absorption coefficient we can use a formula of the ratios of the peak to peak amplitudes at 800 nm and 760 nm using linear fit, hemoglobin oxygen saturation = 1.54 - 0.76 x (amplitude of 760 nm/ amplitude of 800 nm).

The differences in absorption coefficients of hemoglobin as well as water absorption coefficient can be seen in Figure 4. Human tissues are predominately comprised of water. However, the wavelengths utilized in our experiments are below water absorption coefficients, ranging from (760-800 nm). Hemoglobin has a high absorption coefficient in the near infrared range with the absorption dependent on oxygenation levels [48]. Of importance, with light at 800 nm (the isobestic point) there is no difference in the absorption coefficients of oxy- and deoxygenated hemoglobin while there is a difference at 760 nm. The significant difference between oxygenated and deoxygenated hemoglobin absorption coefficients in the near infrared spectral range will allow increased sensitivity in signal acquisition despite attenuation by chromophores such as melanin in the skin. Melanin does have a high absorption in the near infrared range but consists only of a thin layer in the superficial dermis with the absorption spectra that has a mildly flat course at the wavelengths we are measuring [49]. Additionally using the peak amplitudes of two wavelengths (760 and 800 nm) that are close together we can limit the effects of melanin's absorption on our measurements [50]. Additional chromophores, such as cytochrome c, will be in the tissues we are evaluating but their absorption coefficients are minimal in the wavelength range we are utilizing [51].
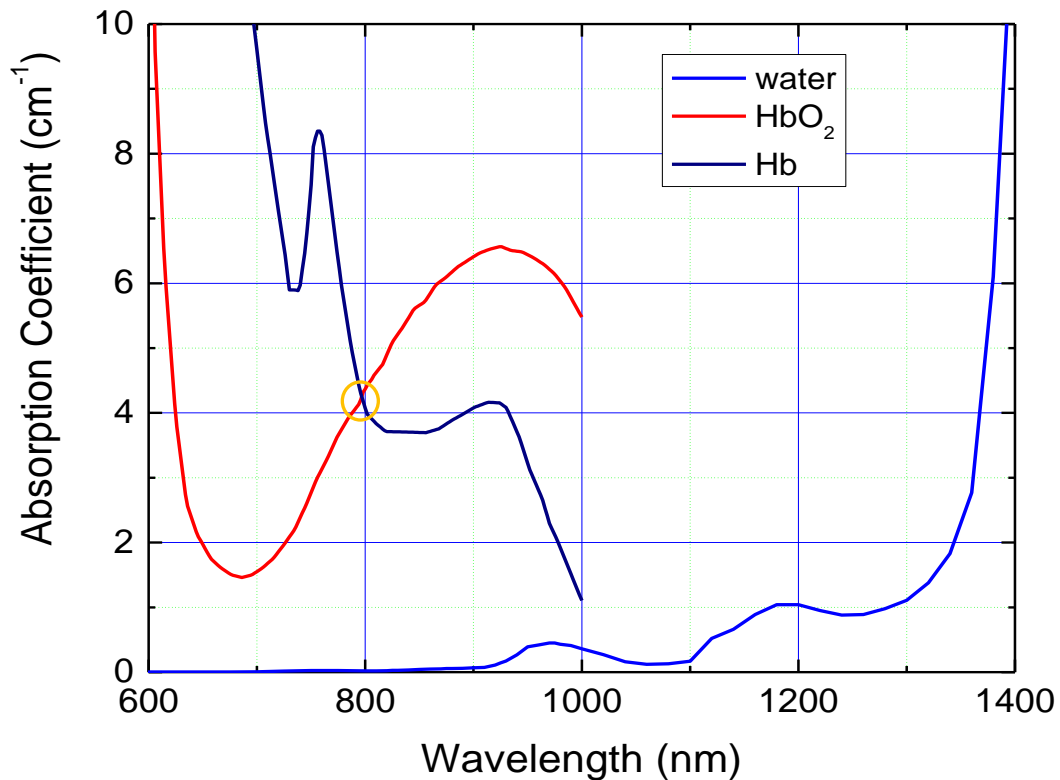
Figure 4: Absorption coefficients spectra of oxygenated/deoxygenated blood and H_2O [52] with the isobestic point at 800 nm (yellow circle).

By comparing the absorption amplitude differences with 800 nm and another wavelength such as 760 nm in which amplitude varies with hemoglobin oxygenation (Figure 5) we can predict hemoglobin oxygen saturation. This is done by algorithms using the exponential slope or amplitude of signal obtained at these two wavelengths. The selection of 760 nm was based on the large difference between of oxygenated and deoxygenated Hb (Figure 4), while 800 nm serves as a reference wavelength. The plotted estimates of varying oxygenation saturation levels based on absorption coefficients (Figure

5) correlated well when compared to in-vitro sheep blood (Figure 6) measured in cuvettes [52]. Additional animal studies were performed in which venous oxygen saturation was varied by changing the fraction of oxygen with inhaled gas (FiO2) and measuring the cerebral venous oxygen saturation with our laser optoacoustic device that demonstrated accurate measurements between invasively obtained SSS venous samples and our device [53–56].
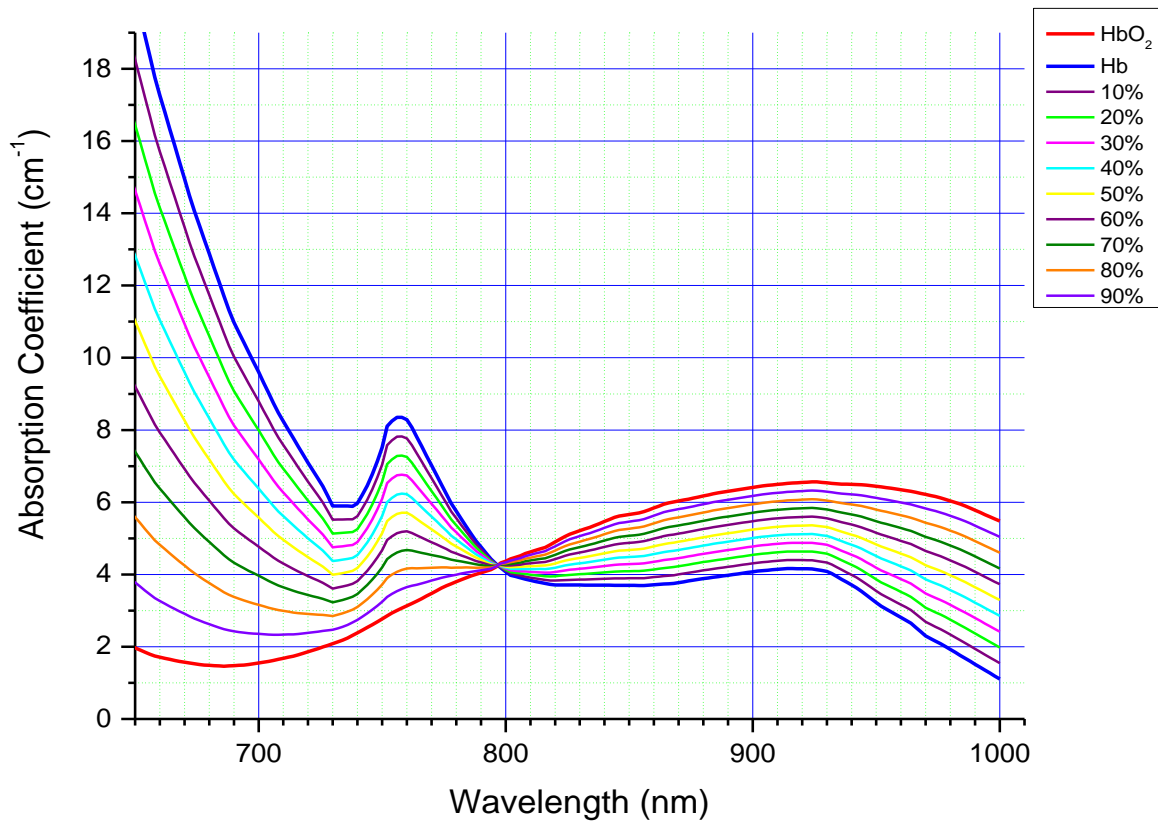
Figures 5: Spectra of absorption coefficients of Hb plotted with 10% oxygenation increment. The spectra are obtained using the data from Prahl [57].

Since our device gives us both temporal and spatial data, we can locate a large cerebral vein such as the SSS. Additionally neonates have open fontanelles which accommodates for the growing brain and are uncovered by calvarium/skull bone with only

a thin layer of covering soft tissues. The anterior fontanelle is the largest in human neonates and is open for several months while the posterior fontanelle is smaller in size. Since this fontanelle is not covered by bone (Figure 7), only by a thin soft tissue overlying the SSS, it allows for excellent acquisition of the SSS signal.
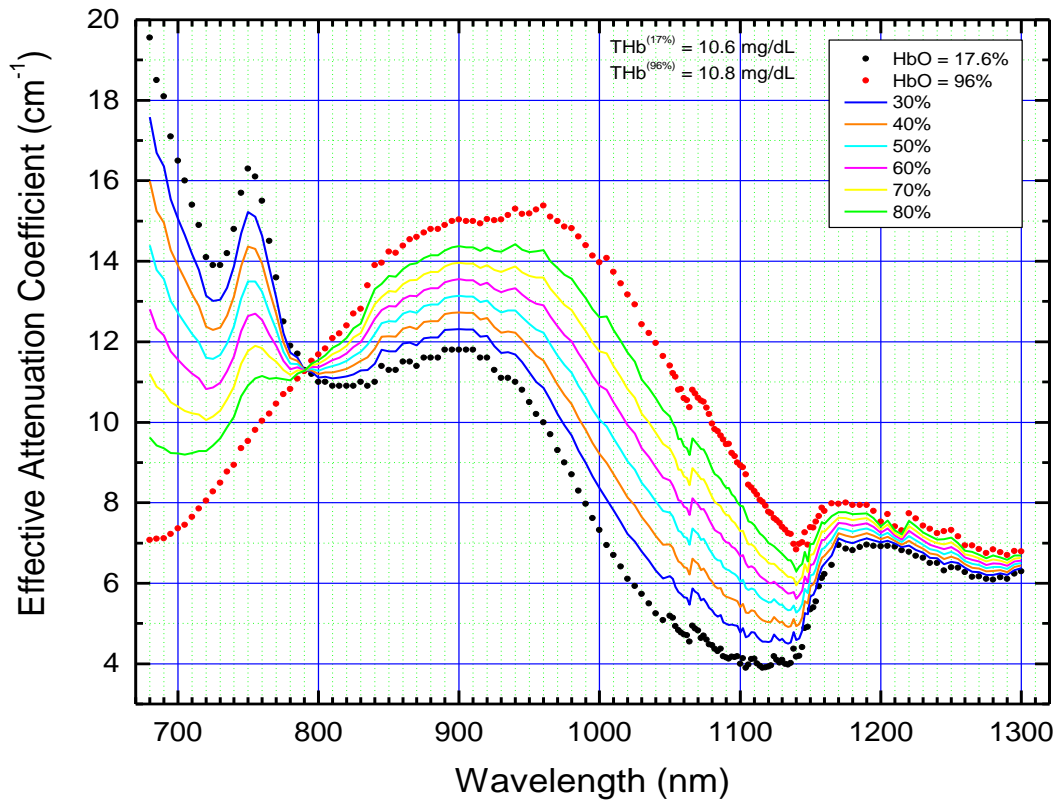
Figures 6: Effective attenuation coefficients at different hemoglobin saturation [52].

Our project will utilize a non-invasive optoacoustic device to measure cerebral venous oxygen saturation in neonates through the anterior and posterior fontanelles. By using the optoacoustic technique we were able to benefit from high optical contrast as well as minimal scattering of ultrasound waves [58]. Initial studies were performed on a plastisol phantom which was designed based on neonatal head CT measurements of the

16

SSS and overlying soft tissues. Subsequently we obtained measurements from neonates in the neonatal intensive care unit at UTMB.
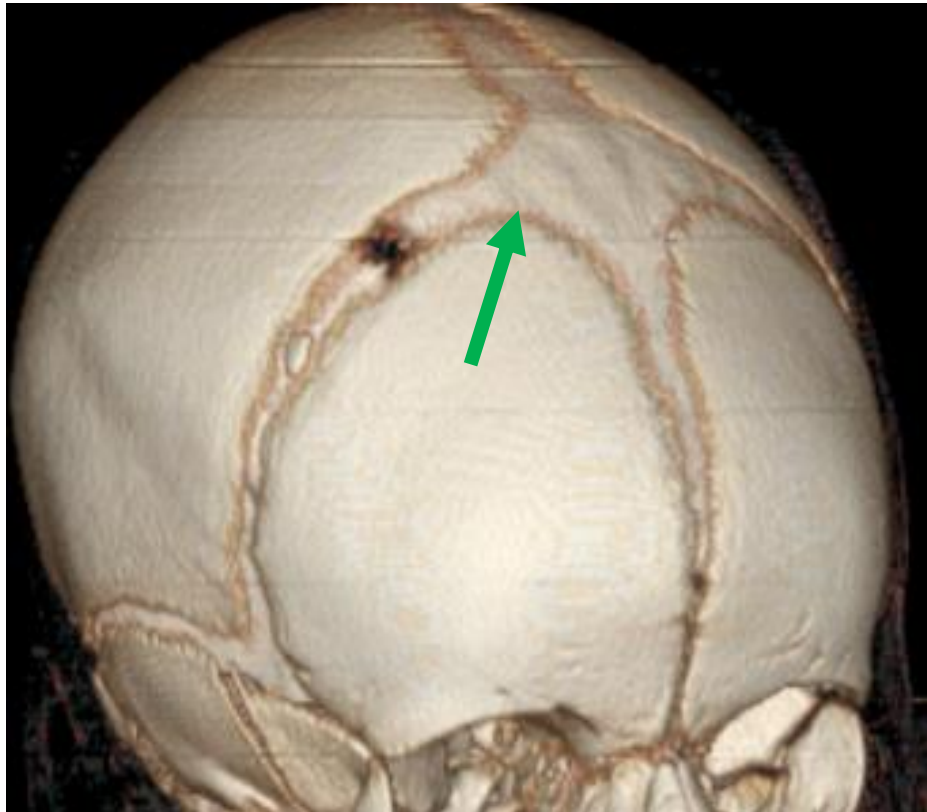
Figure 7: Neonatal 3D CT head demonstrating open fontanelle between skull bones (green arrow).

Optoacoustic Detection: Reflection and Transmission Modes

As per Beers-law, a light is attenuated exponentially within an absorbing medium, meaning as light passes through a medium, energy is absorbed by the medium and results in a reduction in light intensity [38]. This exponential growth of optoacoustic signal will depend on the effective attenuation, based on the combination of tissue scattering and absorption coefficients. We will be testing two different laser modes in these studies, which differ primarily in the placement of the optoacoustic detector. In both modes, the laser enters the tissue and is attenuated by the tissue. In reflection mode, the ultrasound records the pressure wave reflected back to the position of the laser (Figure 8). In transmission mode, the transmitted light travels through the tissue and the ultrasound pressure wave is recorded opposite of the laser pulse (Figure 9). A wide-band ultrasound probe was calibrated to receive the appropriate signal amplitude produced from hemoglobin by using a central frequency that can evaluate for the attenuation coefficient of hemoglobin in the range of near-infrared light. Our probes are manufactured so that it can perform both in a reflection and transmission mode.

Pre-amplifiers were also calibrated to obtain a signal-to-noise ratio (SNR) adequate to provide an acceptable optoacoustic signal. The optoacoustic probes were designed to be hand held and small in order to facilitate use by medical providers in the confined areas that are commonly encountered in the hospital such as neonatal or pediatric intensive care units.
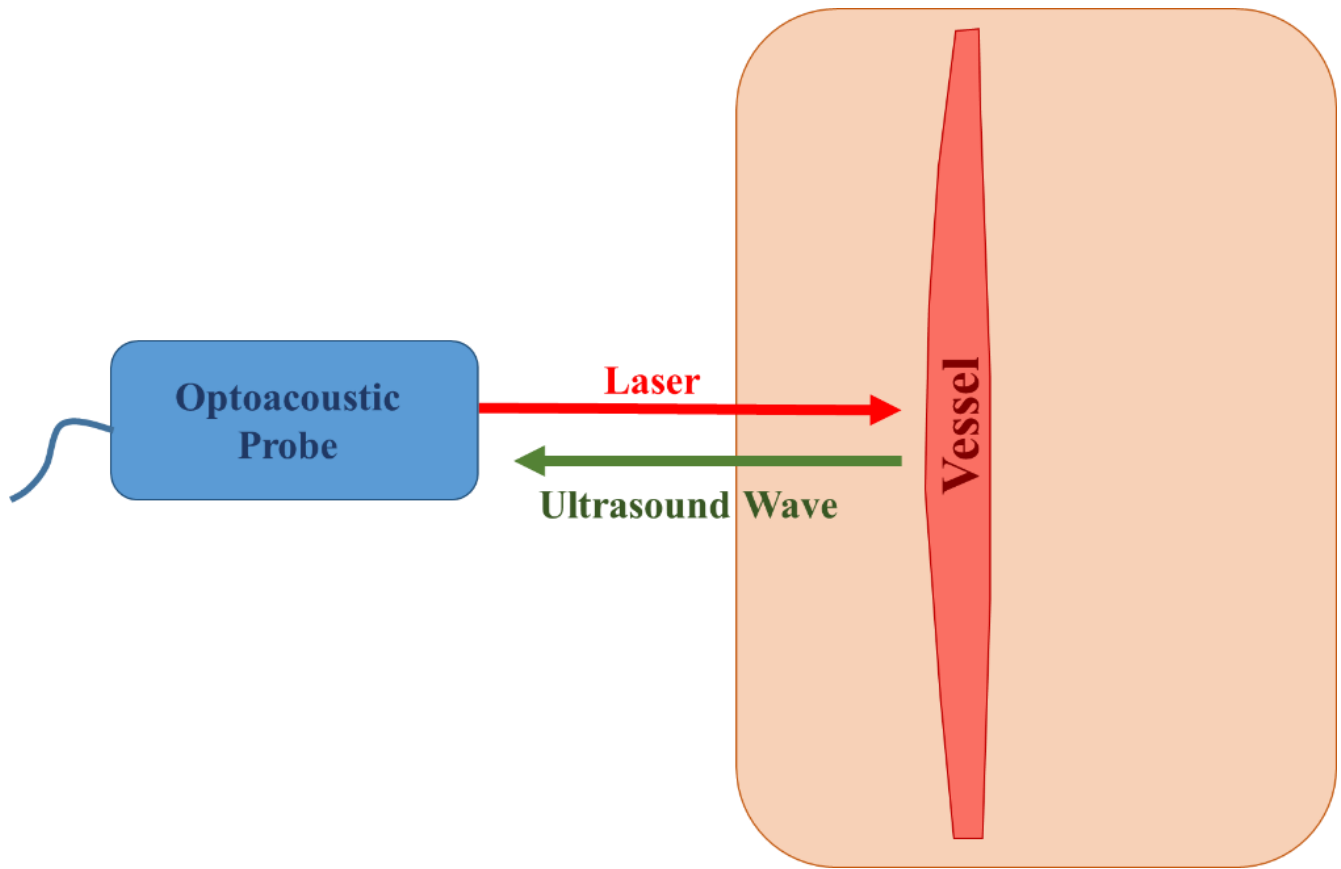
Figure 8: Representation of laser optoacoustic measurements in reflection mode.
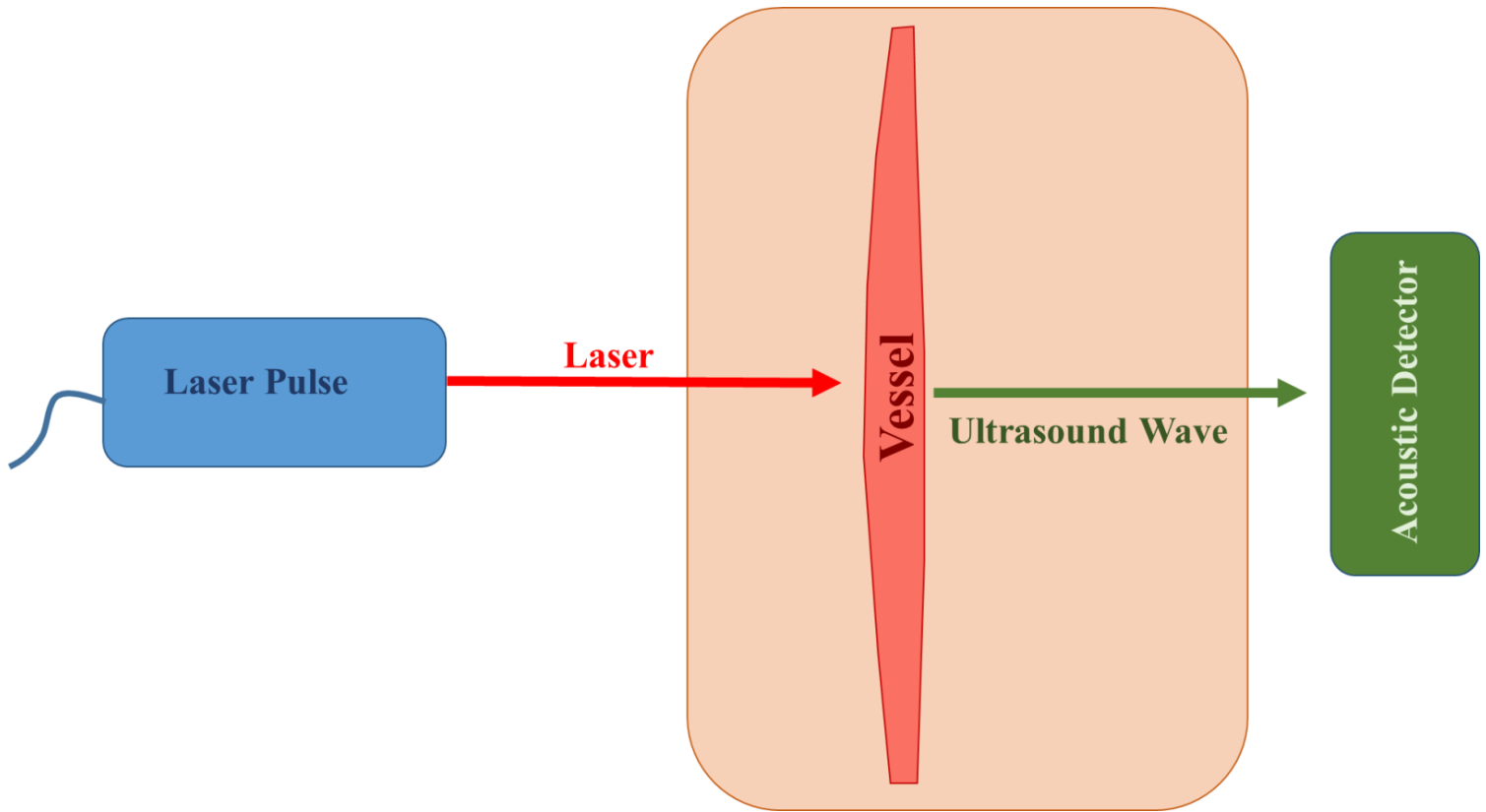
Figure 9: Representation of laser optoacoustic measurements in transmission mode.

Optoacoustic Setup

Our optoacoustic setup is based on a laser diode system which was developed and built using our experience with optoacoustic systems utilizing optical parameter oscillators (OPOs) [59–63] (Opolette HE, Opotek Inc., Carlsbad, CA) as a pulsed laser light source. OPO-based optoacoustic systems are large devices (Figure 10A) and not easily

maneuverable in small confines. The optoacoustic system our lab developed uses a multi-wavelength fiber-coupled laser diode and allows us to perform optoacoustic monitoring in small confines (Figure 10B). Additionally, we implemented a high pulse repetition rate, fast acquisition, and processing software that accommodates for decreased motion artifacts compared to the OPO-based system.

The laser diodes emit pulsed light in the near-infrared range (680 – 1064 nm) with short 130 ns duration at 1 kHz pulse repetition rate. By using such short pulses the stress-confined conditions allow for high resolution, while high pulse repetition rate and provide fast measurements. Our software was designed in order to acquire and process signals very quickly for both the reflection and transmission modes [59,60]. The fast signal acquisition and processing allows us to obtain real-time continuous cerebral venous oxygen saturation and provides both single measurements as well as continuous monitoring of blood oxygen saturation.
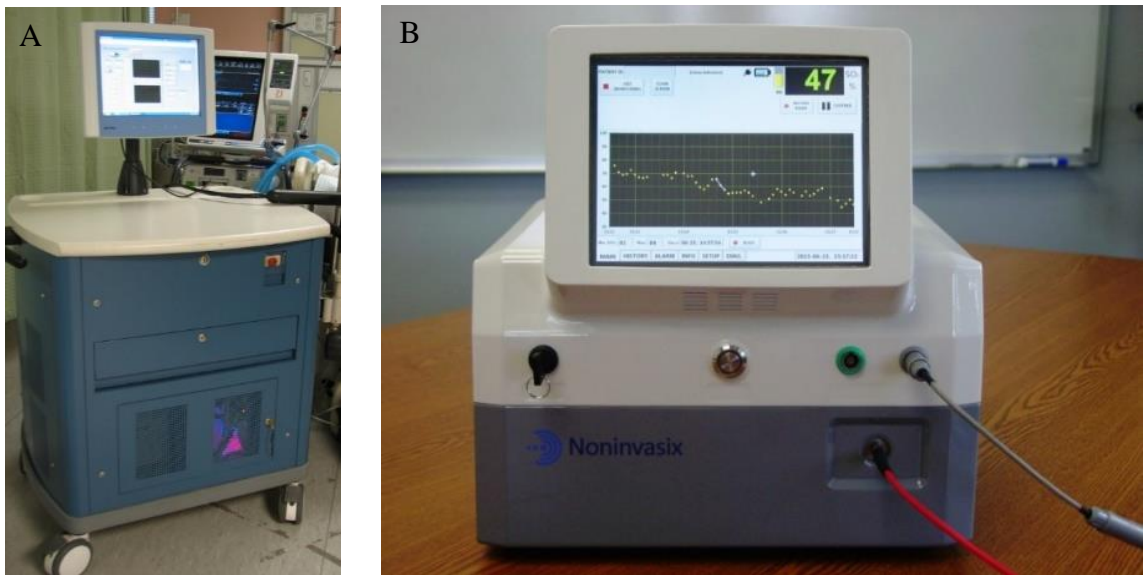
Figure 10: A) OPO based optoacoustic system and B) a laser diode- based optoacoustic system.

We obtained measurements in the reflection mode over the anterior and posterior fontanelles. Transmission mode was used with light introduced at the frontal bone and signal acquisition obtained from the occiput region at the back of the neonatal head. Post processing analysis was performed with OriginLab© data analysis and graphing software which was used to design our graphs and process data.

Chapter 3 NEONATAL PHANTOM DESIGN

Superior Sagittal Sinus

In order to manufacture a neonatal phantom we evaluated the normal dimensions of the SSS within neonates via imaging. Multiple imaging modalities were reviewed to consider which could provide the most accurate assessment of neonatal SSS dimensions such as computed tomography (CT), MRI, magnetic resonance venography (MRV) and US. There were many neonatal head ultrasounds available at our institution that provided excellent imaging of the neonatal SSS anatomy (Figure 11) but there were concerns due to differences in operator technique, overlying pressure from the US probe altering normal overlying soft tissues/SSS morphology and off axis measurements. Both MRI and MRV (Figure 12A and B) provided excellent detail of the SSS anatomy and overlying soft tissues but were limited in the number of studies available due minimal usage in neonates. CT was finally selected as the modality of choice due to amount of studies available, excellent visualization of both soft tissues/bones and reformatting availability in multiple sagittal/coronal/axial views (Figure 13A) allowing for accurate measurements of the SSS (Figure 13B) and overlying structures.
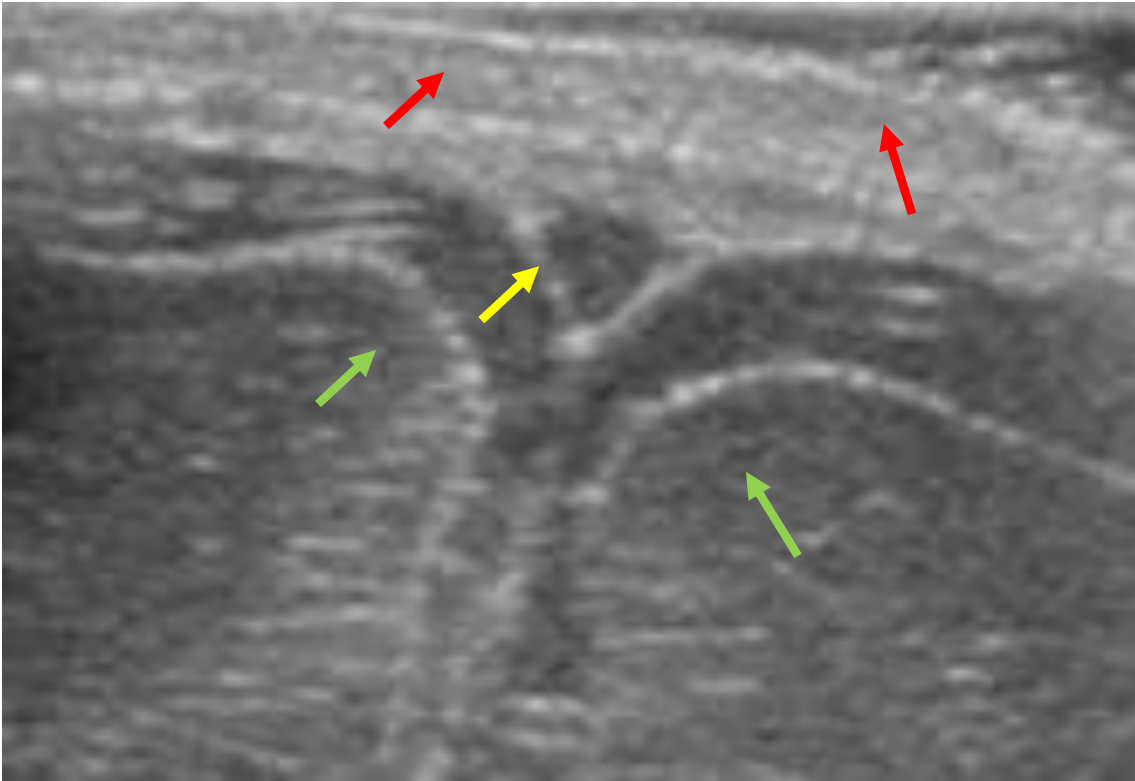
Figure 11: US transverse image of a neonatal SSS (yellow arrow), subcutaneous tissues (red arrows) and brain parenchyma (green arrows).
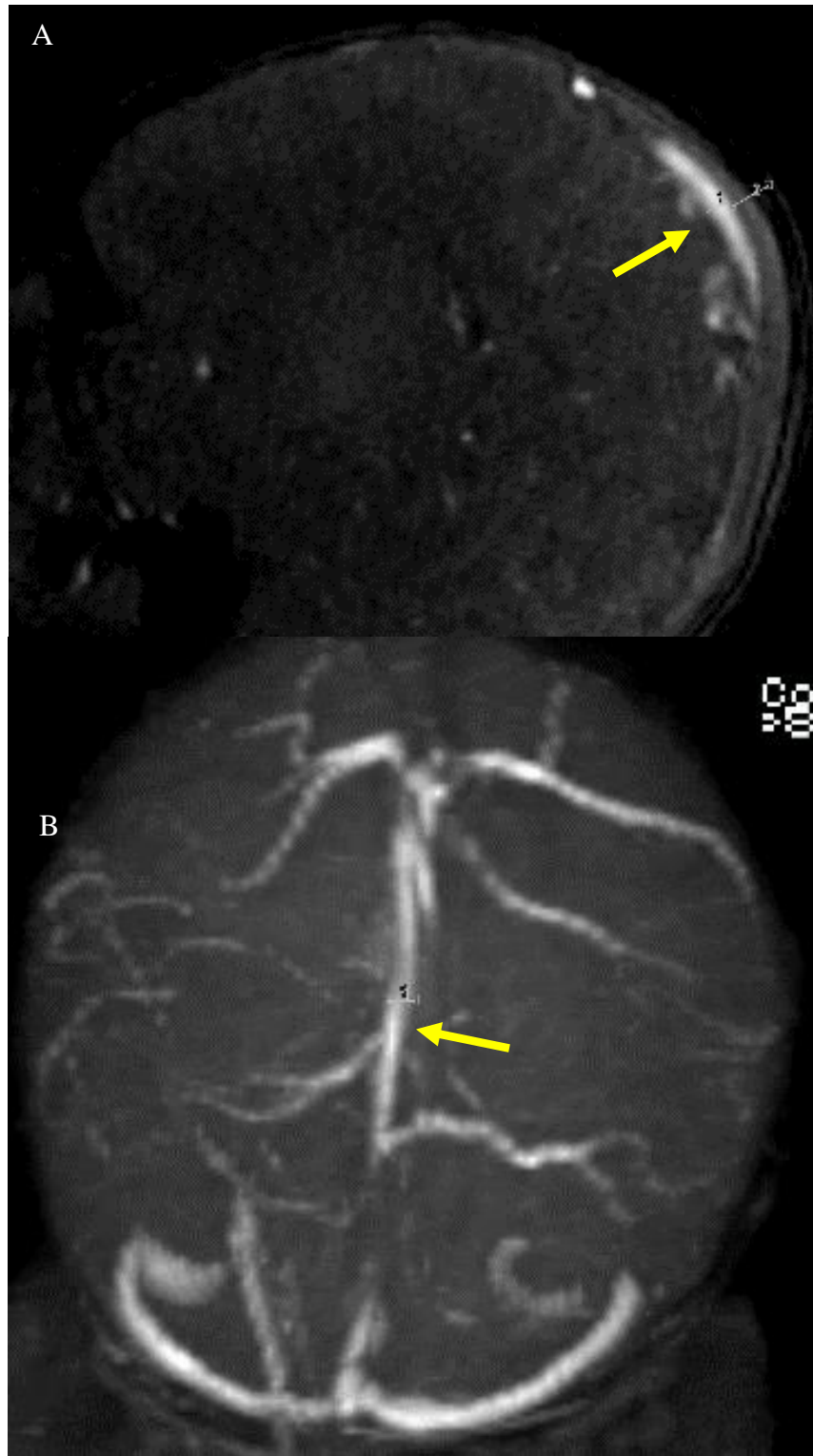
Figure 12: A) MRV sagittal and B) coronal images demonstrating SSS dimensions (yellow arrows).
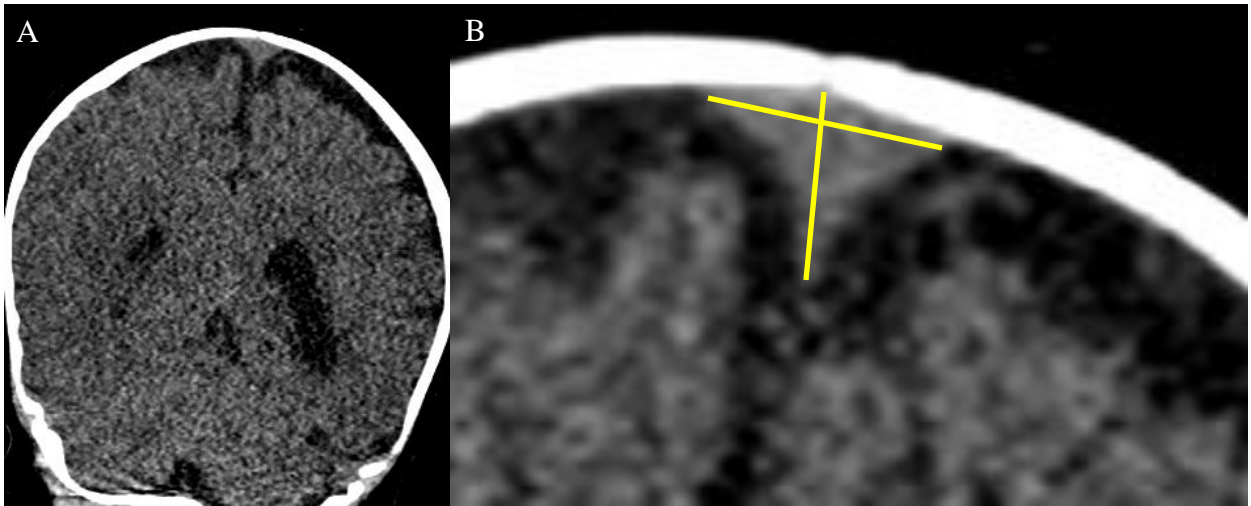
Figure 13: A) CT coronal image of neonatal head and B) Small field of view brain window demonstrating SSS dimensions (yellow lines).

We subsequently performed a retrospective review of neonatal head computed tomography (CT) over a span of 4 years after obtaining approval by the Institutional Review Board of UTMB. Over 40 CT heads were reviewed with approximately 25 selected for measurements and the others excluded due to multiple factors including subgaleal hematomas, caput succedaneum, calvarial fractures, intraparenchymal hemorrhage, craniosynostosis or other abnormalities that would alter either neonatal SSS dimensions or overlying soft tissue measurements. The most frequently encountered abnormalities were scalp swelling or hematomas which caused variable thickening of the overlying soft tissues (Figure 14).
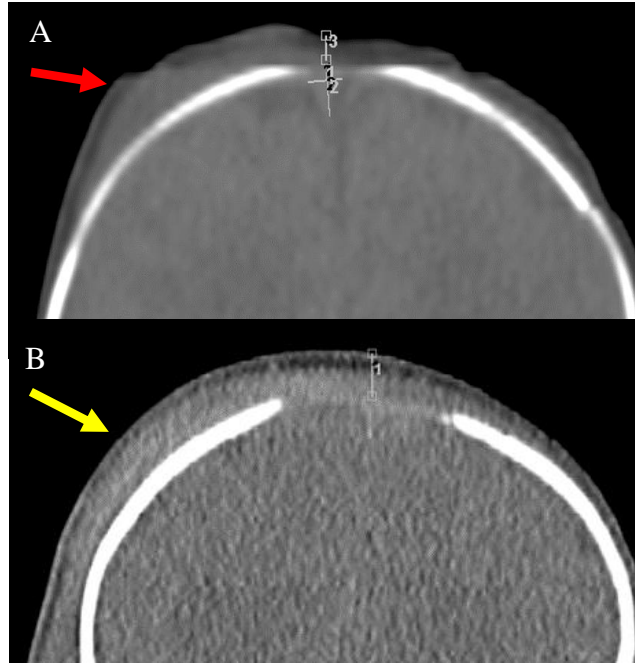
Figure 14: CT coronal images with small scalp hematomas over the A) posterior fontanelle (red arrow) and B) anterior fontanelle (yellow arrow) in a different neonates causing variable soft tissue thickening over the fontanelles.

We obtained measurements at three locations consisting of the anterior fontanelle, posterior fontanelle and occiput. The fontanelles are openings between skull bones which are only covered by soft tissues and can be easily located on physical examination as "soft spots". The anterior fontanelle is located anteriorly between the frontal bone and bilateral parietal bones and has been used for years with ultrasound to investigate cerebral anatomy and pathology in neonates [64] due to lack of overlying bony calvarium that would significantly attenuate any acoustic signal. The anterior fontanelle measures approximately 2.1 cm (average of the anterior-posterior and transverse dimensions) [65] although variations between ethnicities have been seen [66] and appears to enlarge with increased gestational age. The posterior fontanelle is on average smaller than the anterior fontanelle but also can be accessed with US to evaluate intracranial structures due to minimal overlying bone [67]. The occiput was measured near the location of the superior sagittal

sinus just prior to draining into the confluence of sinus. The relation of the anterior/posterior fontanelles, confluence of sinuses and SSS can be well visualized on sagittal CT images (Figure 15).
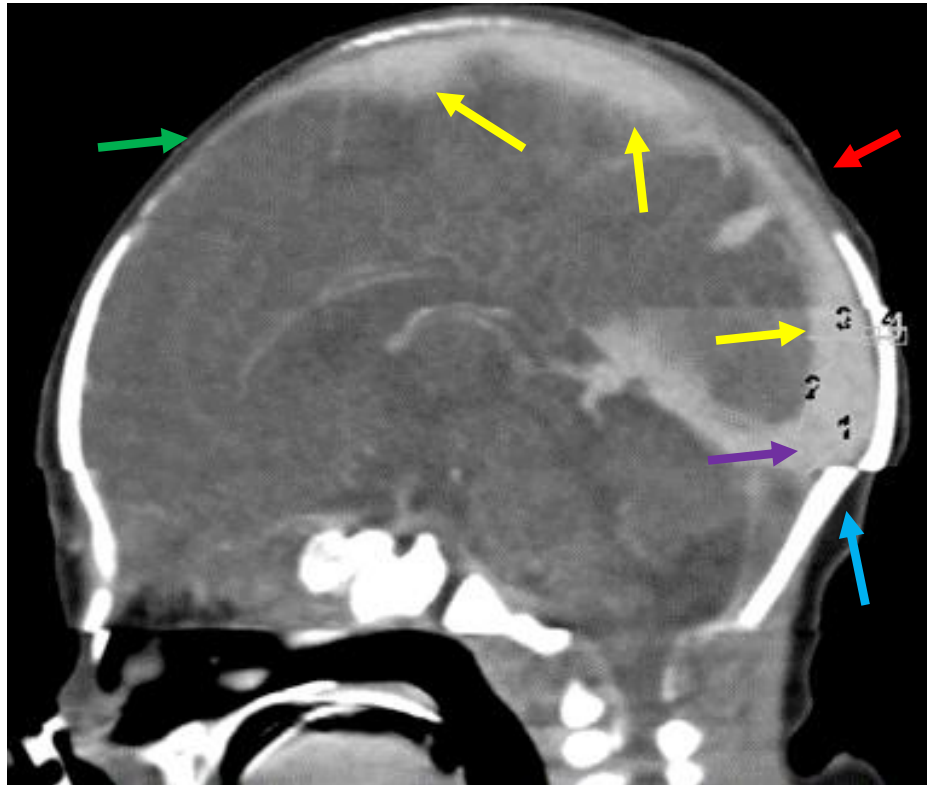
Figure 15: Sagittal CT head demonstrating the relationships of the anterior fontanelle (green arrow), posterior fontanelle (red arrow), bony occiput (blue arrow), SSS (yellow arrows) and confluence of sinuses (purple arrow).

We were able to obtain an average and standard deviation of the SSS height and width at the levels of the anterior/posterior fontanelles and occiput. We also measured the overlying skin/bone to aid in designing of a model of the SSS and overlying structures that might affect signal acquisition. Measurements from the anterior/posterior fontanelle and occiput of 0-2 week neonates are presented in Table 1, with additional measurements in

neonates from 2-4 weeks presented in Table 2. Table 3 demonstrates the average measurements for all three locations. The average SSS height and width at the anterior fontanelle was 5.5 and 6.2 mm, respectively. The average SSS height and width at the posterior fontanelle was 5.9 and 8.1 mm, respectively. The average overlying soft tissue depth at the anterior fontanelle was 2.3 mm and at the posterior fontanelle was 3.5 mm.

0- 2 weeks

Age	Sex	AF SSS Height (mm)	AF SSS Width (mm)	AF Skin to SSS (mm)	PF SSS Height (mm)	PF SSS Width (mm)	PF Skin to SSS (mm)	PF Bone Width	Occiput Region SSS Height (mm)	Occiput region SSS Width (mm)	Occiput Region Skin (cm)	Occiput Region Bone Width	Head Length (mm)	Head Width (mm)
6d	f	5.2	6.6	2.3	5.6	7.0	3.8	0.0	3.9	5.0	4.7	4.5	118.0	98.0
9d	m	5.9	7.8	2.0	5.0	11.0	2.3	0.0	3.5	4.6	6.6	5.8	104.0	90.0
0d	m	7.0	7.8	2.2	4.1	8.3	5.0	2.2	4.6	6.3	5.4	2.1	121.0	94.0
0d	m	3.5	6.1	2.0	5.3	5.7	3.0	1.8	4.0	6.7	6.8	3.8	117.0	101.0
2d	f	6.3	6.2	1.8	5.7	5.2	2.4	0.0	4.1	5.3	5.7	4.0	117.0	101.0
1d	m	5.2	4.8	3.0	10.0	11.2	4.6	2.2	5.6	8.6	7.1	3.1	115.0	105.0
1d	m	5.2	4.2	1.5	6.5	9.8	3.5	0.0	3.5	9.1	5.2	3.5	115.0	87.0
0d	m	4.0	5.3	2.2	3.7	6.5	2.1	0.0	4.3	4.8	5.2	2.2	113.0	92.0
1d	m	4.5	6.6	2.4	5.1	7.8	4.0	0.0	4.0	10.2	5.3	3.1	118.0	86.0
9d	m	4.5	4.0	3.2	6.5	8.1	2.7	0.0	5.3	8.2	5.6	2.4	120.0	98.0
0d	m	4.7	6.0	1.0	6.0	4.7	6.4	0.0	3.4	5.2	6.8	4.3	108.0	90.7
2d	f	5.5	5.7	1.8	6.4	7.8	4.9	0.0	4.2	4.2	5.0	2.1	118.0	104.0
2d	m	5.2	7.3	2.6	4.7	8.6	2.6	0.0	5.4	6.4	5.2	2.9	117.0	93.0
0d	m	4.7	8.3	5.8	8.2	15.5	3.0	0.0	6.0	7.7	5.2	3.0	122.0	100.5
1d	m	6.5	8.9	2.4	5.7	7.3	5.2	0.0	7.0	5.4	5.6	3.0	118.0	95.0
6d	m	7.7	5.9	1.2	5.3	6.5	1.5	0.0	4.5	5.4	4.3	2.9	110.0	88.0
1d	f	4.0	4.2	1.0	6.3	6.6	3.4	0.0	5.0	6.3	4.4	2.6	118.0	91.0
3d	f	6.7	5.0	1.7	4.6	6.0	3.0	0.0	7.1	6.5	3.4	2.0	108.0	88.0
3d	m	4.0	5.7	2.4	8.7	9.2	2.9	0.0	5.1	7.8	3.1	2.0	108.0	86.0
7d	f	4.9	7.3	2.9	5.0	8.8	3.9	0.0	5.1	5.1	4.7	3.7	113.0	91.0
Mean		5.3	6.2	2.3	5.9	8.1	3.5	0.3	4.8	6.4	5.3	3.2	114.9	94.0
Standard Deviation		1.1	1.4	1.0	1.5	2.5	1.2	0.7	1.1	1.7	1.0	1.0	5.0	6.0

Table 1: Measurements of anterior/posterior fontanelle, occiput, SSS and overlying tissues in neonates (0 - 2 weeks).

Age	Sex	AF SSS Height (mm)	AF SSS Width (mm)	AF Skin to SSS (mm)	PF SSS Height (mm)	PF SSS Width (mm)	PF Skin to SSS (mm)	PF Bone Width	Occiput region SSS Height (mm)	Occiput region SSS Width (mm)	Occiput region Skin (mm)	Occiput Region Bone Width	Head Length (mm)	Head Width (mm)
15d	m	7.4	7.4	4.4	7.8	7.7	5.0	0.0	4.1	4.3	5.4	2.9	119.0	99.0
28d	f	5.3	7.2	2.0	4.2	6.7	2.5	0.0	4.3	6.0	5.5	2.3	123.0	91.0
16d	f	4.2	4.7	2.2	5.1	7.3	2.0	0.0	3.7	8.0	4.0	1.5	123.0	100.0
20d	m	9.8	4.0	2.0	7.0	11.6	3.4	0.0	9.5	14.0	4.5	2.6	116.0	92.0
29d	f	4.3	7.1	2.5	4.8	6.4	3.6	0.0	5.9	5.6	5.2	3.3	119.0	98.0
Mean		6.2	6.1	2.6	5.8	7.9	3.3	0.0	5.5	7.6	4.9	2.5	120.0	96.0
Standard Deviation		2.4	1.6	1.0	1.5	2.1	1.2	0.0	2.4	3.8	0.6	0.7	3.0	4.2

Table 2: Measurements of anterior/posterior fontanelle, occiput, SSS and overlying tissues in neonates (2 - 4 weeks).

	Anterior Fontanelle SSS Height (mm)	Anterior Fontanelle SSS Width (mm)	Anterior Fontanelle Skin to SSS (mm)
Mean	5.5	6.2	2.3
Standard Deviation	1.4	1.4	1

	Posterior Fontanelle SSS Height (mm)	Posterior Fontanelle SSS Width (mm)	Posterior Fontanelle Skin to SSS (mm)
Mean	5.9	8.1	3.5
Standard Deviation	1.5	2.3	1.2

	Occiput Region SSS Height (mm)	Occiput region SSS Width (mm)	Occiput Region Skin (cm)	Occiput Region Bone Width
Mean	4.9	6.7	5.2	3
Standard Deviation	1.4	2.2	1	0.9

Table 3: Average and standard deviation of the SSS height/width and overlying soft tissues/bones at the anterior/posterior fontanelles and occiput in neonates (0-4 weeks).

Plastisol Phantom

Polyvinyl chloride plastisol (PVCP) tissue phantoms were manufactured at the Center for Biomedical Engineering of UTMB. PVCP (M-F Manufacturing Co., Fort Worth, TX) is a non-toxic moldable plastic used in biomedical optoacoustic studies as it has similar optical and acoustic properties of soft tissue [49,68–71] and less limitations compared to polyacrylamide gels or agar phantoms. Additionally the speed of sound of PCVP was found to be within 15% of that encountered in human soft tissue [69]. PVCP consists of monomers which after heating can be poured into a mold and cools to a solid state. During the cooling process a white dye is mixed into the PCVP liquid at a concentration to acquire the same scattering properties of soft tissues that have been documented in prior biological tissue optical reviews [68]. The PCVP phantom has the following optical properties (μ_{eff} = 1.5 cm^{-1}, μ_s' = 2.5 cm^{-1}, and μ_a = 0.27 cm^{-1}) in which administration of a white coloring dye provided similar optical properties to skin and adipose tissue, with a low absorption but high scattering property [71,72]. Once cooled the mold can be removed, easily handled and altered by cutting if necessary. Our phantoms had a homogenous turbid appearance with constant optical properties Our prior in vivo studies [56] demonstrated a high contrast between blood absorption coefficients and background soft tissues, suggesting that the heterogeneous background signal will be minimal compared to that of signal obtained from hemoglobin.

For our experiments, we manufactured a mold in which we were able to insert a triangular metallic rod with similar dimensions as the neonatal SSS based on our radiological review and overlying depths similar to the skin superficial to the anterior and posterior fontanelles. After cooling the mold we removed the triangular rod and were then left with a SSS cavity in which we could instill a naphthol green/intralipid (discussed below) solution with similar absorption and scattering characteristics of oxygenated hemoglobin. A smooth interface was encountered in our phantoms which is similar to the

interface visualized between skin/air in a neonatal scalp. The final plastisol phantom was considered a representative neonatal model due to the comparable measurements to that of a neonatal SSS as well as similar overlying soft tissue thickness at the anterior and posterior fontanelles.

Naphthol green and Intralipid Solution

We made naphthol green and Intralipid (NG:IL) solutions commonly used with phantoms, as these solutions have similar optical properties as soft tissues and blood [68,70,73–75]. Intralipid is a fat emulsion frequently used as an intravenous supplement but is also used in phantoms as a scattering medium [74–76] with minimal absorption. We used a 20% solution (20% lipid per 100 ml solution) that consists of soybean oil, lecithin, glycerin and water. A naphthol green dye was then mixed with the intralipid solution as it is used in biomedical optics due to similar absorption characteristics of tissue [77].

By varying the concentrations of our NG:IL solution we were able to alter the scattering/absorption coefficients of a solution with the following parameters: absorption coefficient of 4.1 cm^{-1}, scattering coefficient of 15 cm^{-1} and effective attenuation coefficient of 15.8 cm^{-1}. We modified our solution to provide a similar absorption coefficient to that seen in a hemoglobin oxygen saturation of 46.8%. A hemoglobin concentration of 15 g/dL was calculated by data based on linear interpolation of molar extinction coefficients between oxygenated and deoxygenation hemoglobin [57,72]. We measured our naphthol green transmission spectra with a standard spectrometer prior to making our combined NG:IL solution (Figure 16). We then evaluated the combined NG:IL solution in spectrophotometric cuvettes to measure absorption under ideal geometry rather than the SSS cavity which was corresponding to blood oxygen saturation of 45.5%, closely approximating the absorption our target of 46.8%.
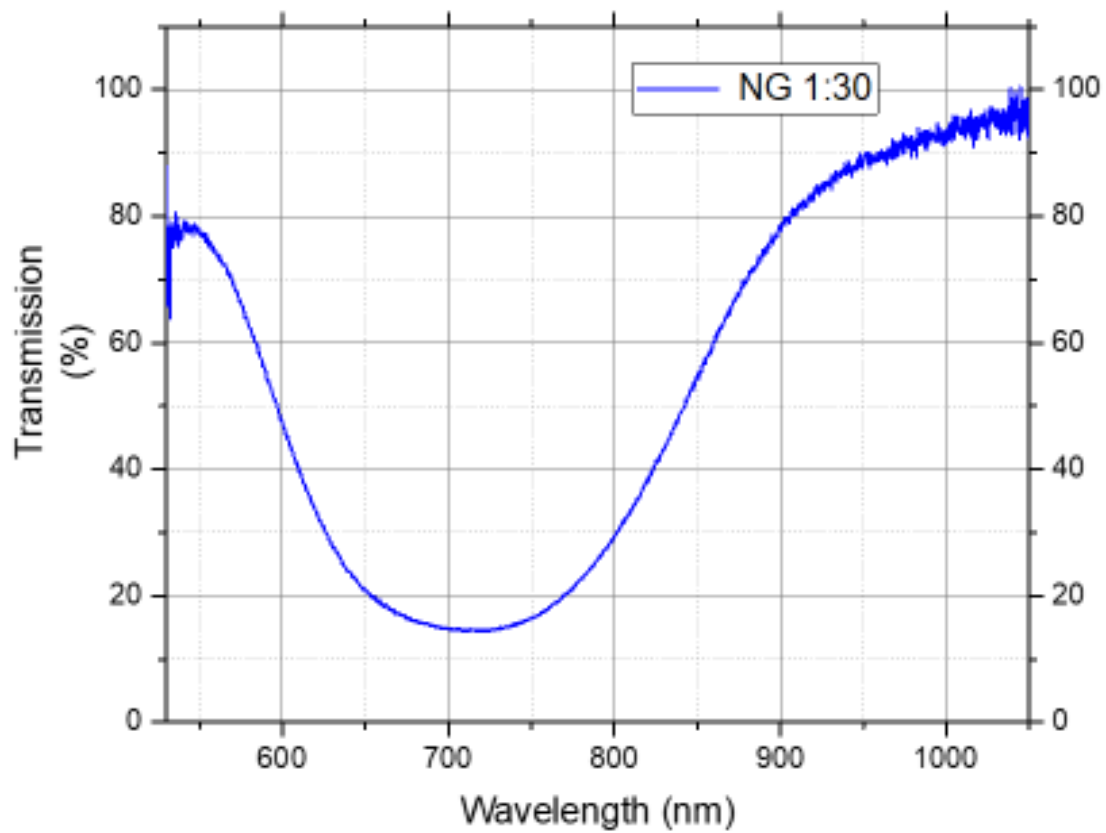
Figure 16: Transmission spectrum of naphthol green dye.

Chapter 4 PRECLINICAL STUDIES

Phantom Setup

For our preclinical studies we prepared our plastisol phantom and NG:IL solution with a scanning system which allows for fixed scanning across our phantoms. The plastisol phantoms had metallic/plastic tubes applied to each end in which the NG:IL solution was instilled into the SSS cavity (Figure 17A). We calibrated the laser fluence prior to examination (Figure 17B) as some energy is lost between our LDS system and the tip of the fiber optic at the end of the optoacoustic probe. The laser parameters (fluence-J/cm^2) that are used in our studies are small and below the maximal permissible exposure (MPE) for ocular injury per the American Standards for Safe Use of Lasers. As such there will be no thermal or mechanical damage to a patient's skin.
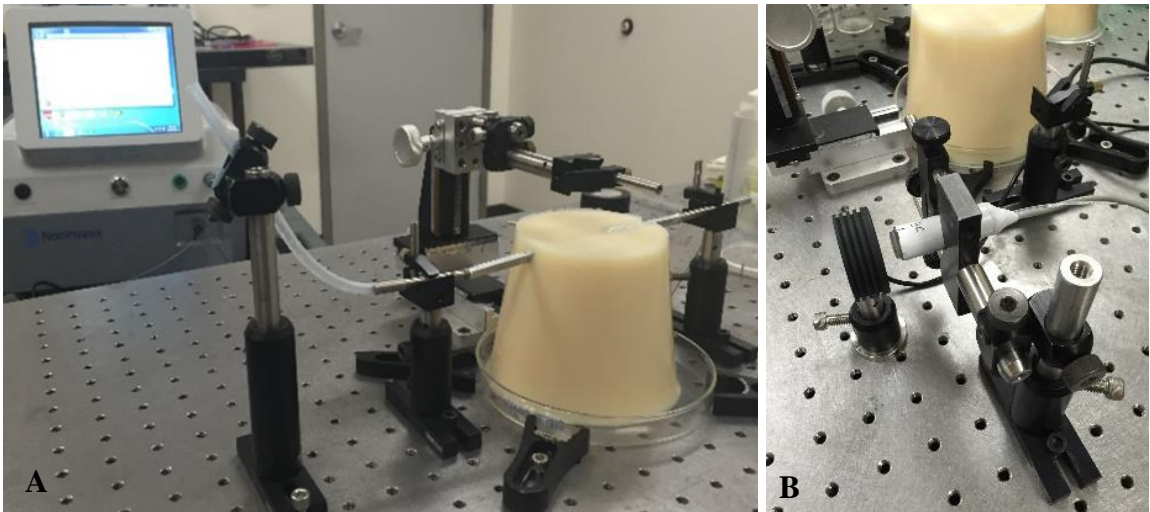
Figure 17: A) Plastisol phantom study setup B) Setup for measurements of laser pulse energy and calibration of the optoacoustic system.

All plastisol phantom studies were performed at the Laboratory for Optical Sensing and Monitoring of UTMB. A small amount of ultrasound gel was applied to the interface of the optoacoustic probe and plastisol phantom which is commonly used in ultrasonographic imaging in order to exclude any interjacent air which would significantly reduce acoustic signal acquisition. For our plastisol phantom studies we evaluated signal acquisition (amplitude) at varying depths corresponding to the overlying soft tissue thickness that would be seen in the neonate at the anterior and posterior fontanelles. We did this to evaluate changes in amplitude due to varying overlying thickness.

Subsequently we performed studies starting at midline of the SSS cavity and at 1 mm increments laterally. Since the geometry of the SSS is triangular we wanted to evaluate what signal amplitude alterations would occur from the thickest part of the cavity at midline to the lateral margins in which the cavity thins out and eventually when signal acquisition would completely fall outside the vessel. Since the cavity itself is not very large (6-8 mm width at the anterior and posterior fontanelles) we were interested in what imaging window would be available for us to acquire stable oxygen saturation measurements for preparation in our later clinical neonatal studies.

Finally our initial NG:IL solutions were created with a solution comparable to that of normal hemoglobin concentration (Hb 15g/dL) with an absorption coefficient corresponding to an oxygen saturation of 46.8%. We then altered our NG:IL solutions to mimic a state of anemia (Hb 7.5 g/dL) while maintaining an absorption coefficient to an oxygen saturation of 46.8% to see if oxygen saturation measurements would be affected. We applied a prototype probe to the neonatal SSS phantom with our NG:IL solution to demonstrate an example of how a typical reflection mode signal amplitude can be obtained (Figure 18). The 760 nm signal amplitude is higher than the 800 nm wavelength signal amplitude corresponding to the higher absorption coefficient that occurs at 760 nm compared to the 800 nm isobestic point (no difference between oxygenated/deoxygenated hemoglobin).
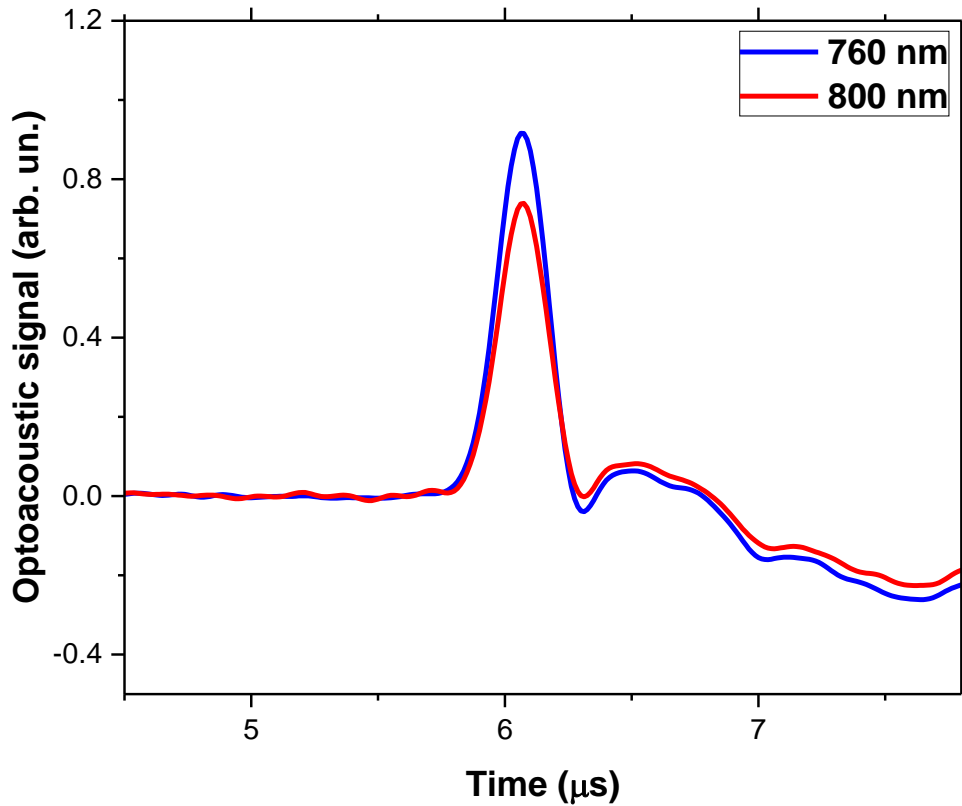
Figure 18: Prototype probe demonstrating signal amplitude in reflection mode.

Depth Studies

For our studies with the neonatal SSS phantoms we used an optoacoustic probe (Figure 19) which was specifically developed to be easier for clinicians to manipulate and use in small confines seen in a NICU setting where neonates are commonly in small incubators limiting movement. A plastic fiber was used in this probe compared to the stiff glass fibers in previous experimental probes which allows for bending and shaping of the fiber to produce an easier hand held tip. A PVLF film element was also utilized in order to provide necessary resolution.

The initial depth studies were performed with a NG:IL solution simulating a Hb concentration of 15 g/dL. We began our depth studies at a depth of 3 mm as this was the minimal depth tolerated by the plastisol phantom before tears in the material could alter signal acquisition. We performed depth studies from 3 mm to 4 mm which demonstrated gradual incremental decreased signal amplitude with increasing depths (Figures 20/21/22). Despite the increased depth attenuating signal acquisition, we were still able to demonstrate stable measurements (Fig 23). The depth study average oxygen saturation measurements obtained with a full concentration was 52.8 % with a standard deviation of 1.6%.

These depths were close to the average overlying soft tissues thickness at the anterior and posterior fontanelles seen with our neonatal CT head review (2.3-3.5 mm). Our depth study findings demonstrate that despite overlying soft tissues attenuating signal with thicker depths we can still obtain stable oxygen saturation measurements, which is important as the soft tissues overlying the anterior and posterior fontanelles will vary depending on gestational age as well as any scalp swelling which may occur due to birth trauma through the vaginal canal.
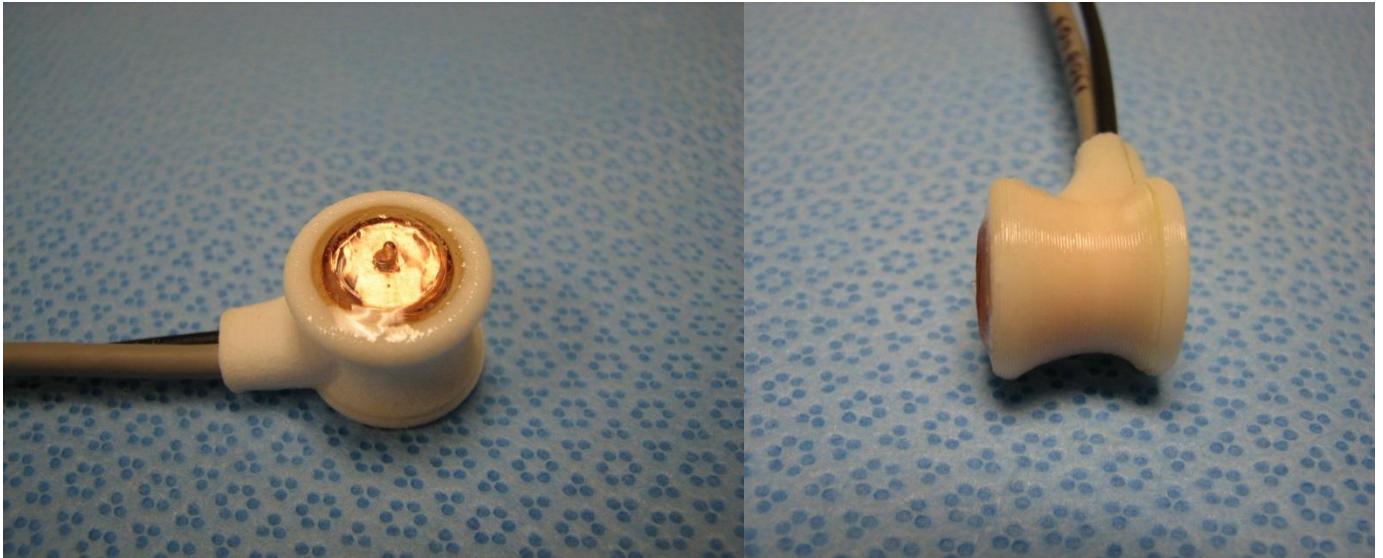
Figure 19: A miniature optoacoustic probe designed for ease of use by clinicians.
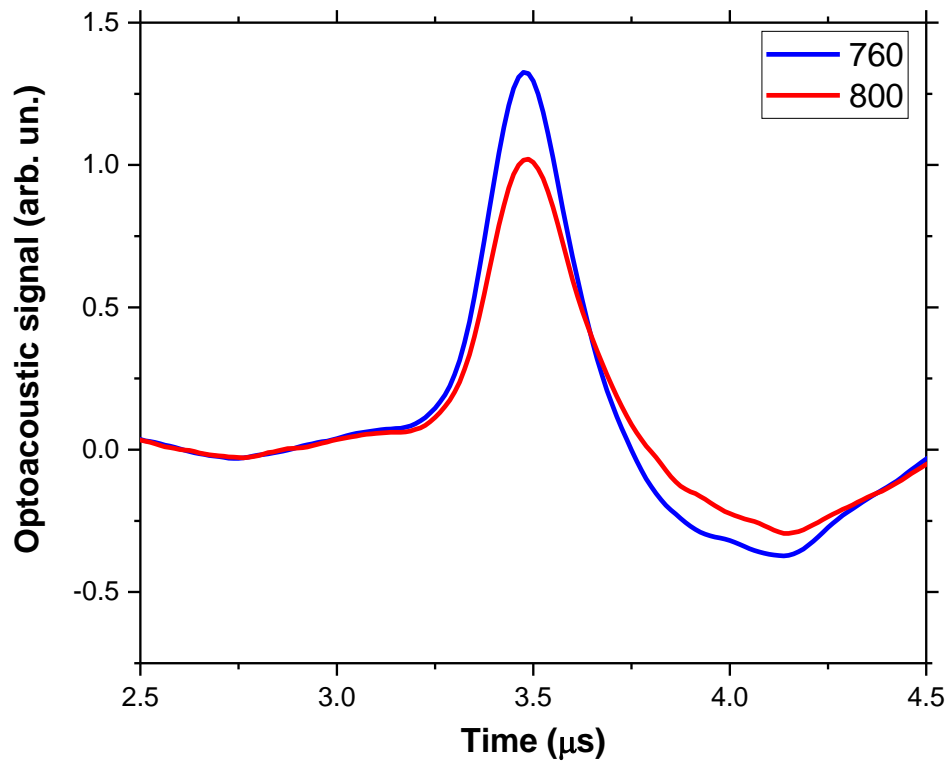
Figure 20: Depth study demonstrating signal amplitude acquired at a depth of 3 mm.
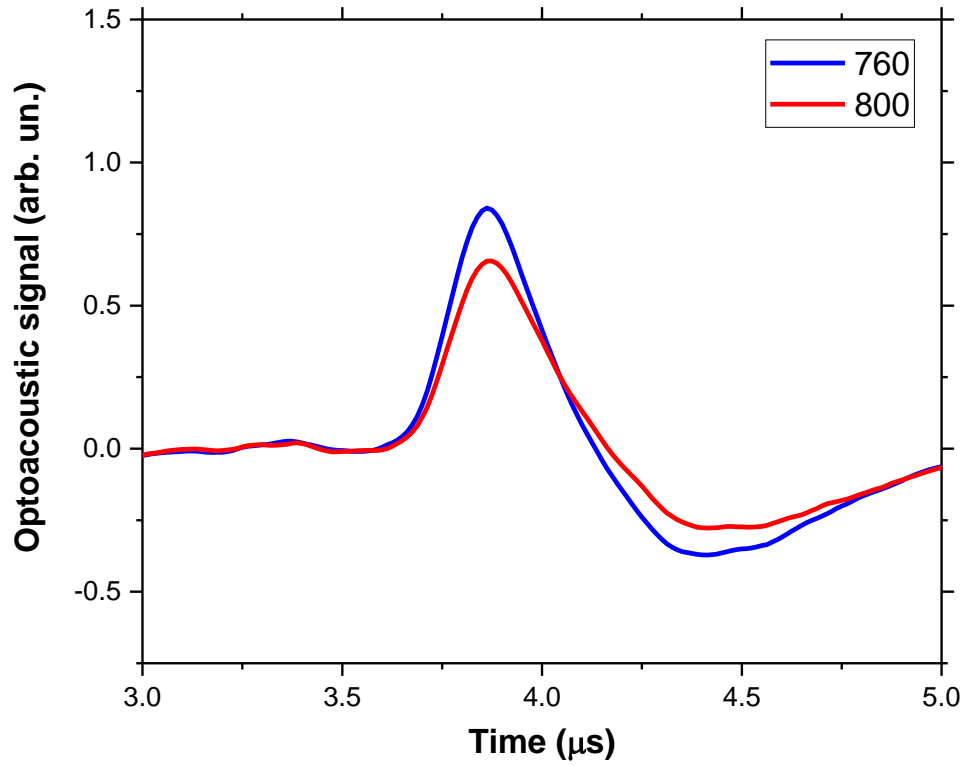
Figure 21: Depth study demonstrating signal amplitude acquired at a depth of 3.5 mm.
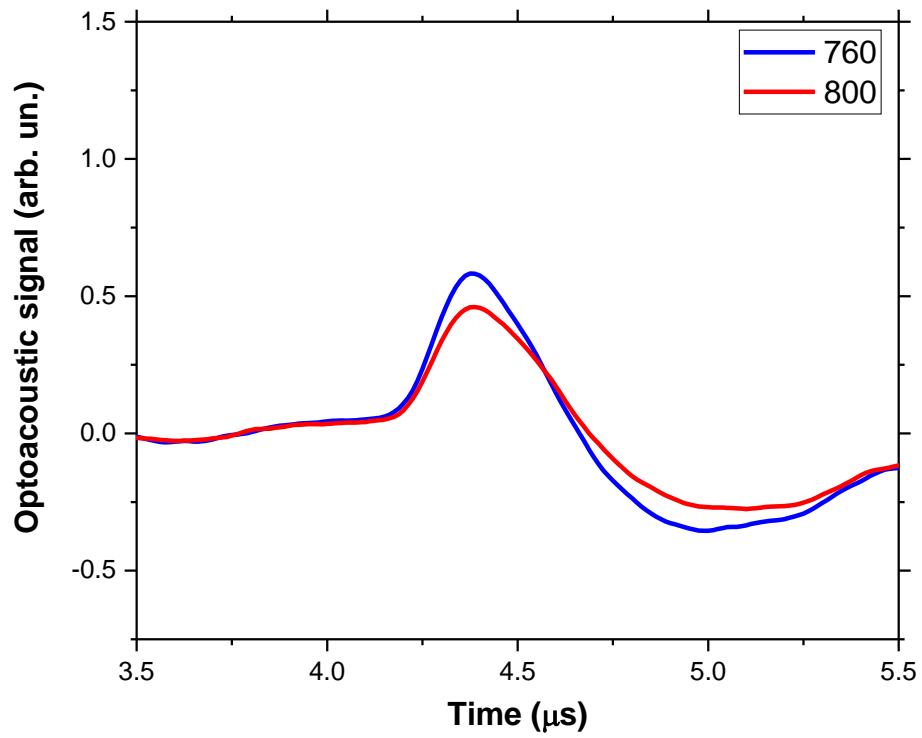
Figure 22: Depth study demonstrating signal amplitude acquired at a depth of 4.1 mm.
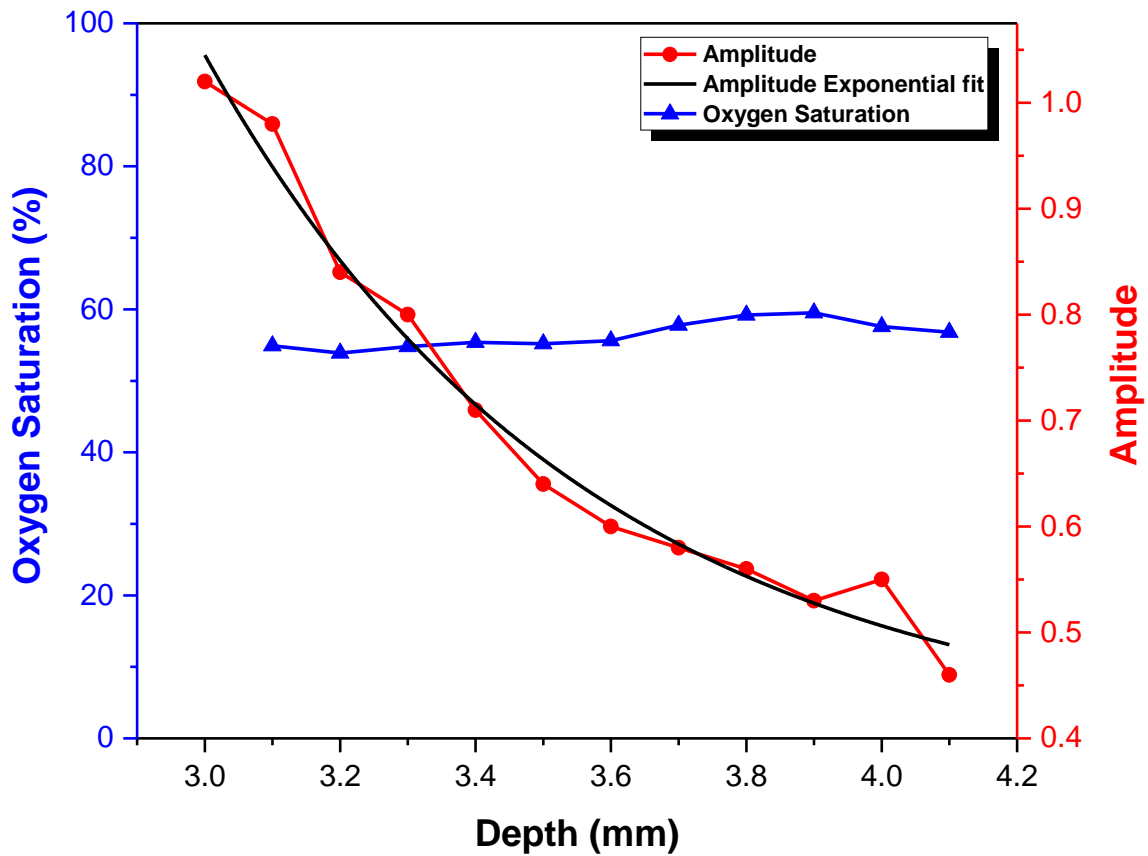
Figure 23: Depth study with preservation of oxygen saturation measurements despite increased depths.

Lateral Displacement Studies

Following the depth studies we performed subsequent experiments to evaluate how the signal acquisition changed with increased lateral measurements from midline. This is important as the SSS has a triangular shape and it is unknown how well signal acquisition can be achieved along the lateral margins where it thinly tapers. We performed studies starting at the midline at three different depths (3, 4 and 5 mm) and then measured signal

at 1 mm increments laterally until signal degraded. The designated midline was at the location near the visualized midline with the highest signal amplitude. At a depth of 3 mm the midline signal amplitude was the highest of all the depths measured and decreased continuously as we measured farther away laterally from midline, as was expected, but the ratios of the 760 nm/800 nm signal remained stable. This preservation of the ratios between the wavelengths allowed us to maintain stable oxygen saturation measurements (Figure 24) despite this gradual continuous decrease in signal amplitude. The measurements were also stable with lateral displacements at increased depths of both 4 mm and 5 mm demonstrating that even starting with decreased amplitudes at midline due to the increased depths, we maintained stable measurements with lateral incremental measurements. This gradual decrease in amplitude at increasing 1 mm lateral increments is best visualized in Figure 25. More notably, the stable measurements were identified within a window measuring approximately 6-7 mm (Figure 24) in width. This corresponds well with our neonatal CT head SSS width measurements at the anterior/posterior fontanelles which measured 6-8 mm. Lateral to this window there was significant variability in signal acquisition, indicating that we have a 6-7 mm window in which we can obtain accurate measurements. The average oxygen saturation measurements obtained within the 6-7 mm window at varying depths were 46.6% at 3 mm, 46.2% at 4 mm and 45.6 % at 5 mm for a total average of 46.1%.
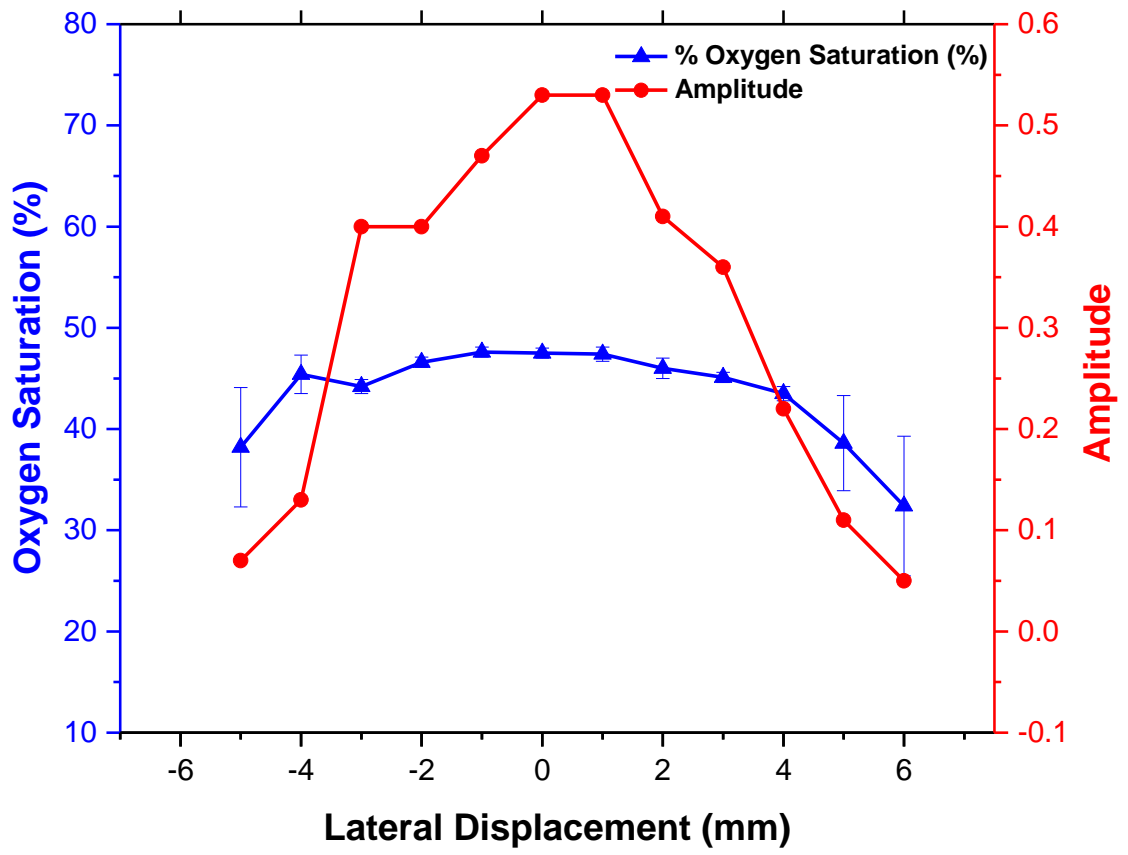
Figure 24: Lateral displacement study with stable measurements within a 6-7 mm window.
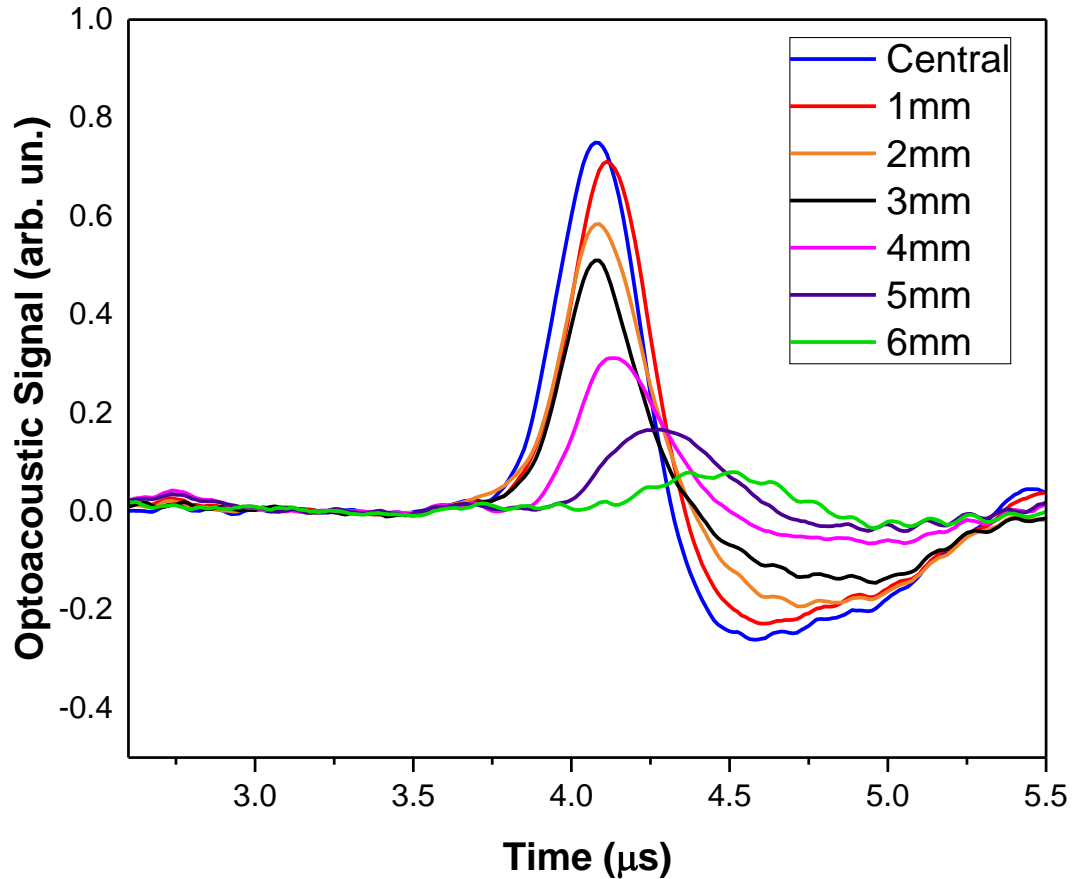
Figure 25: Lateral displacement study with incremental decrease in amplitude from midline.

Normal versus Low Hemoglobin Concentration Studies

Repeat depth studies were performed to simulate an anemic state with a NG:IL solution manufactured to represent a Hb concentration of 7.5 mg/dL (half the normal Hb concentration). Preservation of stable measurements despite the increase in overlying plastisol thickness (Figure 26) was visualized from 2.75 mm – 4 mm. Repeat lateral displacement studies were also performed with the low Hb concentration solution and we were again able to maintain a 6-7 mm window (Figure 27) in which we acquired stable

measurements with significant variability outside this window, like the studies with a normal Hb concentration (15 g/dL). The depth study average oxygen saturation measurements obtained with a full concentration was 47.4% with a standard deviation of 1.3%. The average oxygen saturation measurements obtained within the 6-7 mm window at varying depths were 45.2% at 3 mm, 43.9% at 4 mm and 49.1% at 5 mm with a total average of 46.1%. The increased measurement at 5 mm depth may have been due to multiple NG:IL solution leaks during the study. These results indicate that accurate Hb oxygen saturation measurements do not depend on the Hb concentration, and can be interpreted from neonates with abnormally low Hb concentrations.
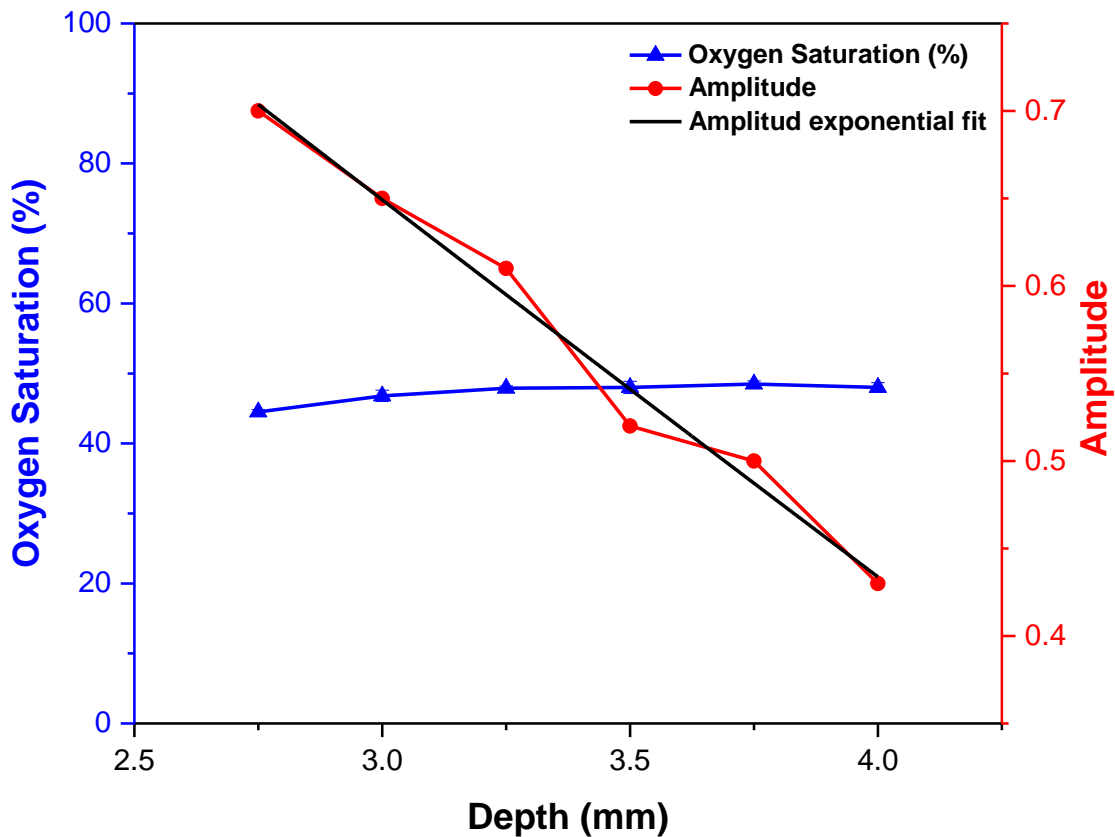
Figure 26: Low hemoglobin concentration depth study with preservation of oxygen saturation measurements.
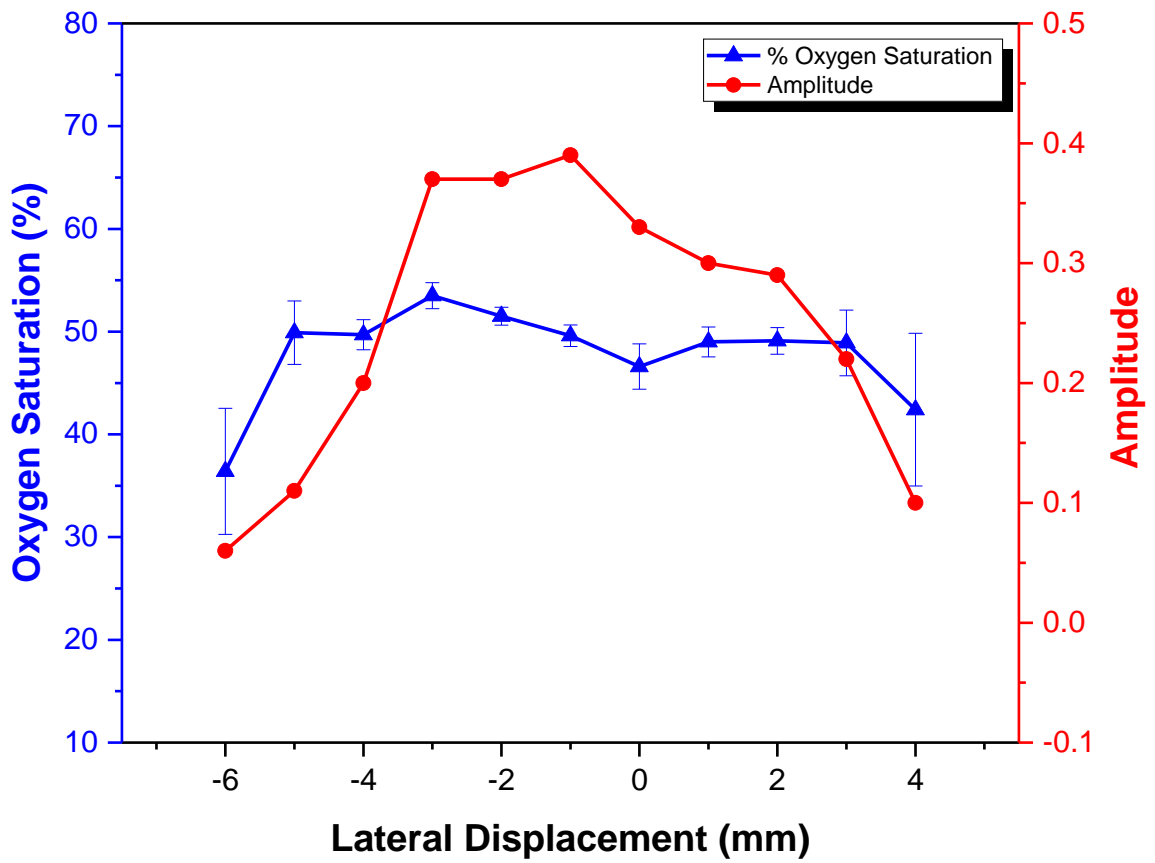
Fig 27: Low hemoglobin concentration lateral displacement study with 6-7 mm window of stable measurements.

Chapter 5 NEONATAL CLINICAL STUDY

Neonatal Selection

The neonatal clinical studies were performed in the UTMB Neonatal Intensive Care Unit (NICU). The clinical protocol for these studies was approved by the Institutional Review Board of UTMB and informed consents were obtained for each subject. Recruitment of neonates was performed by collaborating NICU pediatricians participating in the study. Our laser diode-based optoacoustic system is portable and small enough to easily maneuver in the NICU (Figure 28) in which participating physicians used the device without any issues. A variety of neonates were selected who were clinically stable but varied in sex, gestational age, clinical histories and age at measurements.
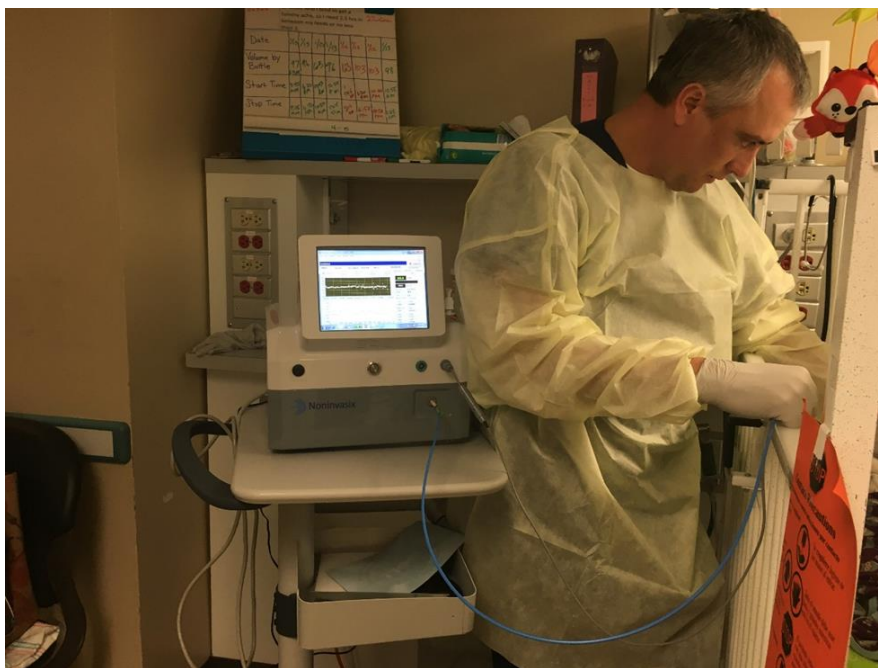
Figure 28: LDS optoacoustic device and probe in utilization by a physician in the NICU that is easily maneuverable within the small confines.

Measurements through the Anterior Fontanelle

Initial placement of our probe at the anterior fontanelle demonstrated optoacoustic signal from both the skin and SSS (Figure 29) with the initial amplitude corresponding to the overlying skin which varied in amplitude likely due to changes in overlying soft tissue thickness and presence of neonatal hair. The SSS depth was calculated by multiplying the time scale (the lower X-axis) by the speed of sound in soft tissue (1.5 mm/μs). The signal amplitude corresponded to a depth that was minimally less than our CT head review but within 1 mm. This was likely related to the pressure from applying the probe to the neonatal head and thinning the soft tissues. Overall this supports the ability of our optoacoustic system to identify and target the SSS for signal acquisition.

We monitored the neonatal SSS venous oxygen saturation measurements continuously and in real time (Figure 30) in a term infant through the anterior fontanelle. Stable measurements at the anterior fontanelle were obtained in different neonates with various clinical histories. Oxygen saturation levels were highly stable when the neonate was not moving but variation would occur if the baby was crying or moving extensively (Figure 31). Fortunately our device can measure oxygen saturation rapidly within seconds and provides stable measurements once the baby is not moving. Despite differences in gestational age, sex, and clinical histories we were able obtain excellent signal acquisition from a premature neonate (Figure 32), again demonstrating the skin and SSS amplitudes which we were able to perform real-time continuous monitoring (Figure 33). The variability in gestation age, weight, gender and clinical histories can be seen in Table 4. The average oxygen saturation measurement acquired with optimal parameters (without baby movement) was 64.5% with a standard deviation of 1.8%.
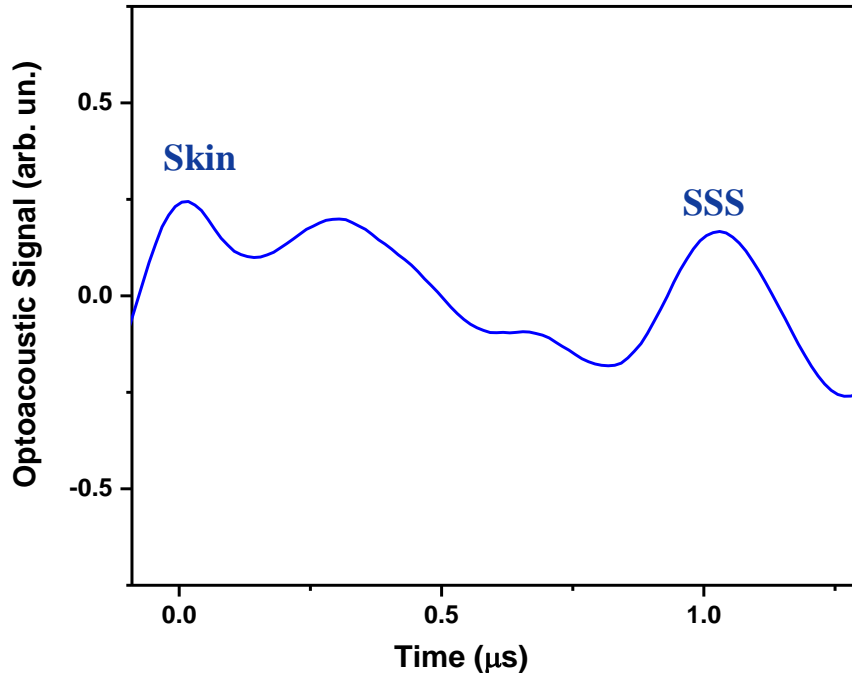
Figure 29: Optoacoustic probe signal acquisition in a term neonate in reflection mode through the anterior fontanelle with initial amplitude (skin) and SSS.
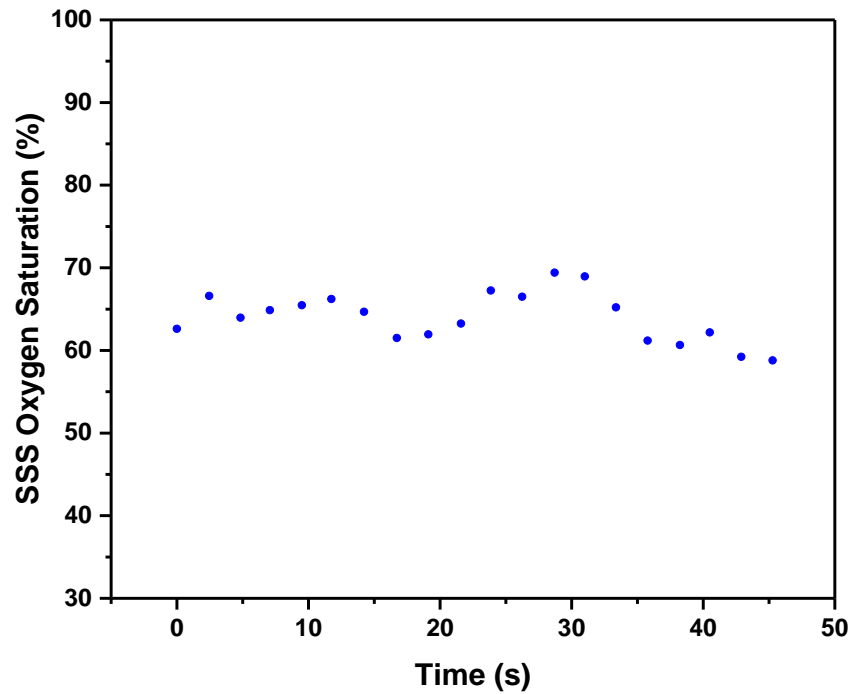
Figure 30: Real time continuous monitoring in a term neonate in reflection mode through the anterior fontanelle.
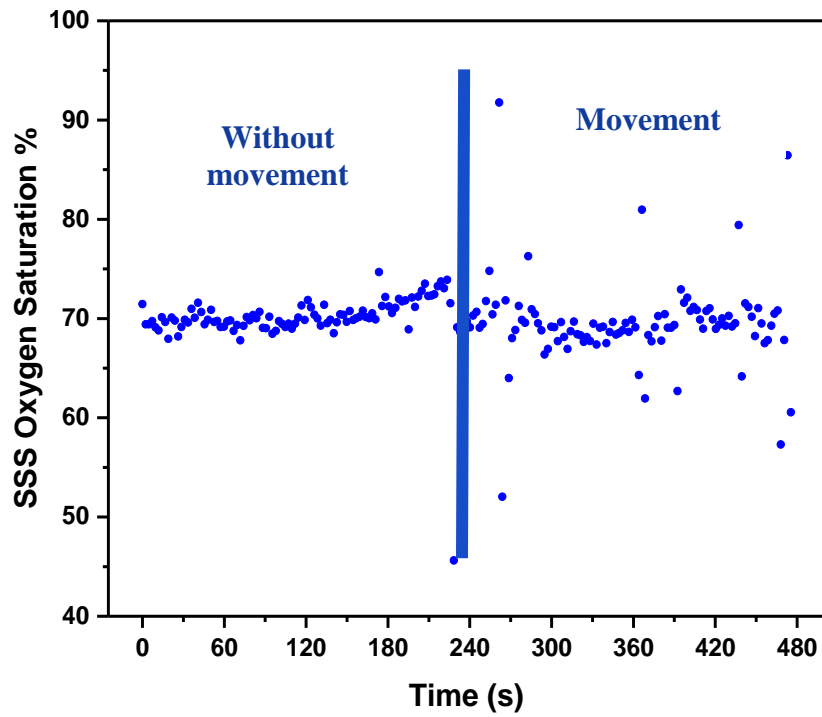
Figure 31: Real time continuous monitoring with and without neonatal head movement.
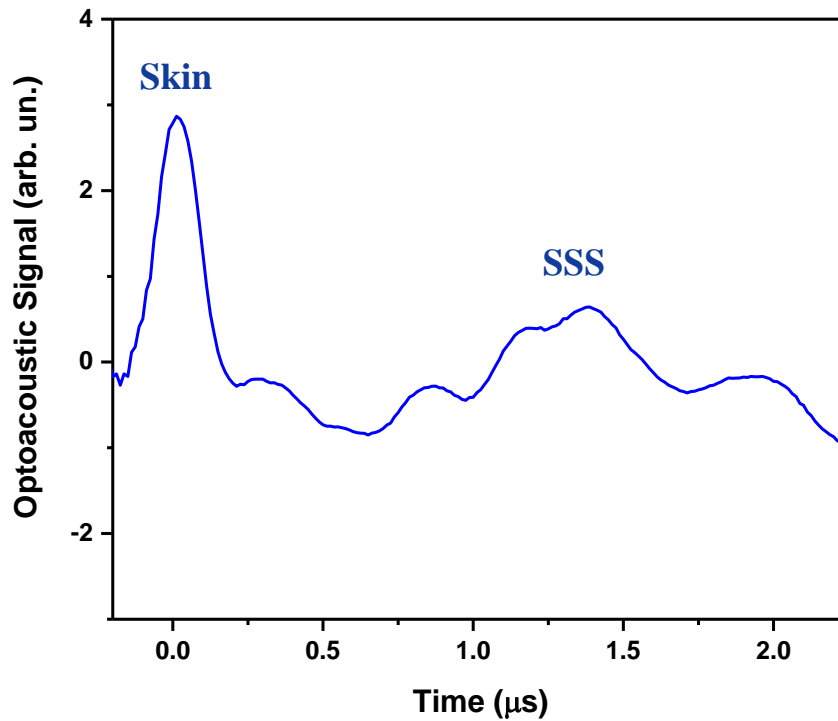
Figure 32: SSS signal acquired from a premature neonate in reflection mode from the anterior fontanelle.
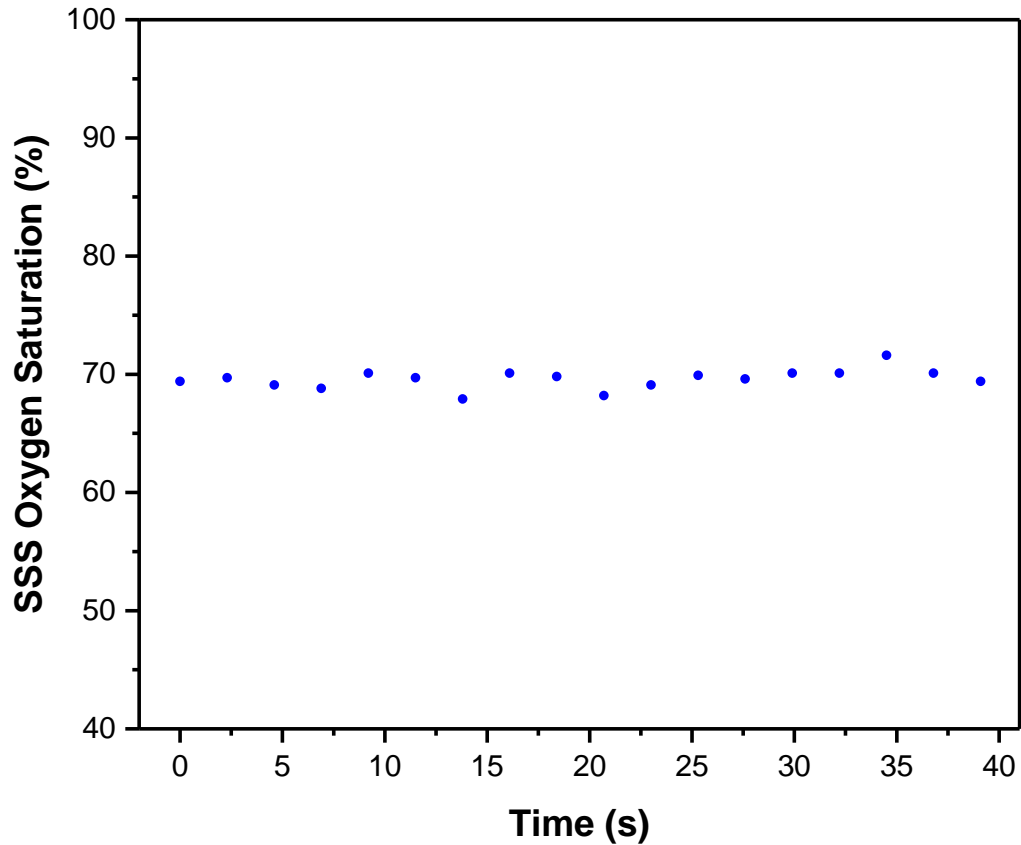
Figure 33: Real time continuous monitoring in a premature neonate in reflection mode through the anterior fontanelle.

Sex	Gestational age at birth	Age at measurement	Birth weight	Weight at measurement	Comorbidities	Oxygenation	Standard Deviation
F	25w 1d	4 months	805g	4710g	ASD, PDA	69.4	2.0
M	37w 1d	9 days	3395g	3325g	VSD, pulm valve stenosis	68.2	0.7
M	38w 2d	2 weeks	3410g	3725g	seizures, post fossa cyst	68.0	0.4
F	38wk 3d	7 days	2940g	3040g	ASD, NEC	68.9	2.9
M	36wk 1d	12 days	3590g	3530g	ASD, SVT	64.0	4.5
F	39wk 3d	2 days	3405g	3335g	Hyperbilirubinemia	64.9	0.8
M	35wk 1d	5 days	1985g	1940g	C-section	60.4	1.9
M	25wk 4d	11 weeks 6 days	800g	2780g	BPD, ROP	62.1	1.2
F	26wk 0d	11 weeks	990g	2015g	BPD, maternal EtOH abuse	60.0	1.8
F	35wk 3d	12 days	3125g	3085g	preterm	59.3	2.7
M	36wk 4d	2 days	2200g	2290g	IUGR, hypoglycemia	71.9	2.2
F	40wk od	11 days	3260g	3315g	ASD, meconnium aspiraiton	59.3	1.1
M	26wk 3 d	9 weeks	1180g	2730g	Pulmonary insufficiency	61	0.9
M	26wk 2d	10wk 5d	970g	3510g	Preterm, ROP	63.6	2.1
M	39wk 5d	1 day	3970g	3970g	hypoglycemia	66.1	2.2
						64.5	1.8

Table 4: Neonatal gender, gestational ages, clinical history and oxygen saturation measurements at the anterior fontanelle.

Measurements through the Posterior Fontanelle

As mentioned previously, the posterior fontanelle is smaller in size then the anterior fontanelle and closes earlier but is still patent in the neonatal time period allowing its use as a possible method for acquiring SSS venous oxygen saturation. We were able to obtain similar signal acquisition when compared to our anterior fontanelle studies with the initial amplitude again representing overlying soft tissues (Figure 34). Additionally, while it was more technically difficult to find the signal due to the smaller opening at the posterior fontanelle and location at the posterior of the scalp, we were still able to provide real-time continuous monitoring of SSS venous oxygen saturation (Figure 35). The average oxygen saturation measurement acquired utilizing optimal parameters (without baby movement) was 66.8% with a standard deviation of 1.3%.
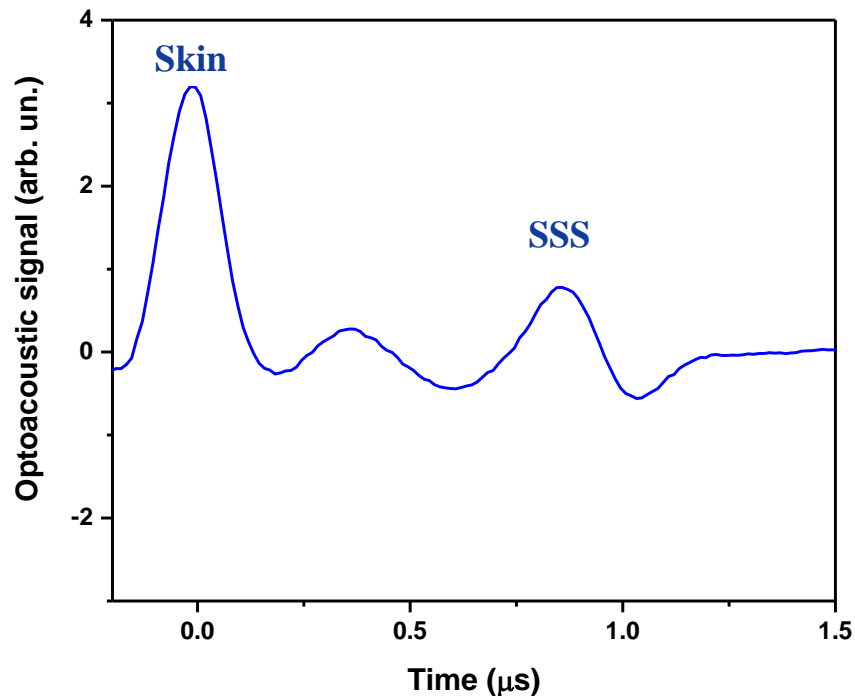
Figure 34: SSS signal acquired from a term neonate in reflection through the posterior fontanelle.
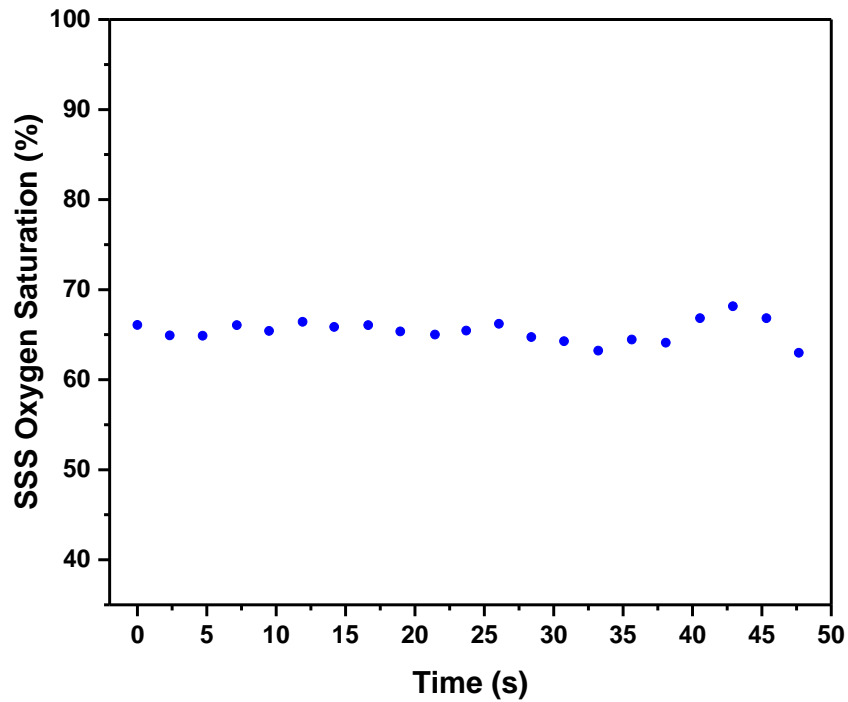
Figure 35: Real time continuous monitoring of SSS oxygen saturation in a term neonate in reflection mode through the posterior fontanelle.

Measurements in Transmission Mode

We performed studies while using the transmission mode which consisted of transmitting laser pulses at the frontal bone with a separate acoustic probe placed at the opposite side of calvarium. This was technically much more difficult when compared to the reflection mode in which the laser and acoustic receiver being embedded within one probe. We were able to obtain signal in several neonates which demonstrated the signal amplitude of the skin, which was received at a later time due to the positioning of the receivers in the different modes (Figure 36). Under optimal conditions were able to obtain continuous monitoring (Figure 37) in a few neonates with the SSS venous oxygen saturation measuring 75.8% with a standard deviation of 4.0%.
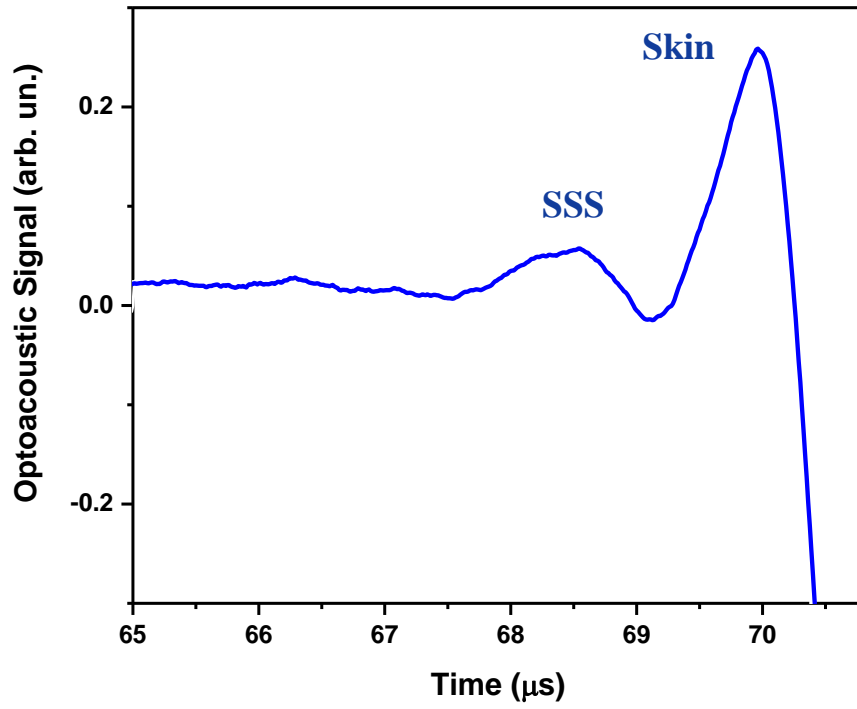
Figure 36: SSS signal acquired from a term neonate in transmission mode.
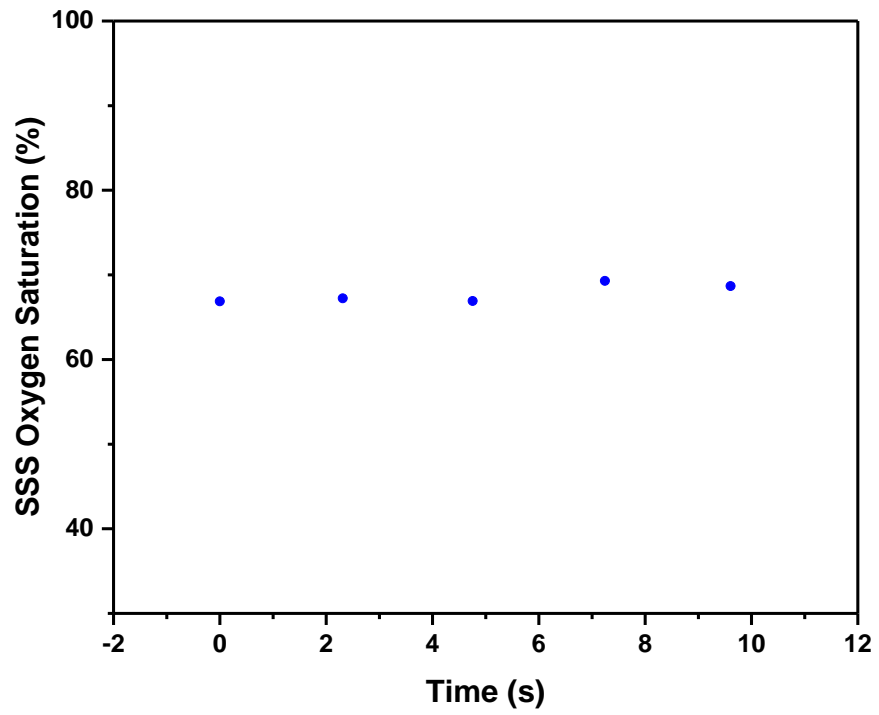
Figure 37: Real time continuous monitoring of SSS oxygen saturation in a term neonate in transmission mode.

Chapter 6 DISCUSSION

Prior studies performed by our lab have demonstrated the ability of optoacoustic signal generation utilizing laser diodes to produce a measurable ultrasound optoacoustic wave to evaluate for cerebral venous oxygen saturation. These initial studies were performed with an optical parameter oscillator (OPO) system [54,55,59–61] in both sheep and a few preliminary neonatal studies. The OPO systems are used to produce lasers at the specific wavelengths needed in our studies but were large and bulky which limits its use in various clinical settings. Our laboratory developed a laser diode based system (LDS) which allowed us to produce the same wavelengths needed but in a smaller, more compact device, allowing for easy maneuverability within small confines. Our studies demonstrated that our newly developed compact LDS system and optoacoustic probe specifically designed for clinical use can acquire signals and measure oxygen saturation from phantom plastisol neonatal SSS phantoms and subsequently in clinically stable neonates.

Pre-Clinical Studies

We were able to successfully evaluate our LDS system on plastisol phantoms designed to represent a neonatal SSS by placing a triangular cavity within the plastisol mold with similar dimensions obtained from a neonatal CT head review. The overlying soft tissue thickness was also obtained from the CT review with the plastisol material representing similar absorption and scattering characteristics of soft tissue. The results from our depth studies demonstrated that we were able to acquire stable oxygen saturation measurements at varying depths despite decreased signal amplitude due to signal attenuation from overlying plastisol thickness. Stable oxygen saturation measurements were present in the depth studies from 3-4 mm with an average oxygen saturation measurement of 52% in normal Hb concentration studies and 47% in our low Hb

concentration studies. These measurements were a close approximation to our intended oxygen saturation of 46.8%. Additionally we identified a 6-7 mm window in which we obtained stable measurements that corresponded well to the actual SSS width documented on our neonatal CT head review. The lateral displacement full concentration studies had very stable measurements with the ranges between 45.6-46.6%. The lateral displacement half concentration studies had a little more variability but still stable with 44-49% measurements and may have been due to leaking of the NG:IL solution in the last study. These findings demonstrate that our neonatal probe could provide both stable and reproducible measurements in our neonatal plastisol phantoms within a window of 6-7 mm from midline. Additionally by using two different solutions to mimic a normal Hb concentration and an anemic state with relative stable measurements we propose that stable measurements can be measured in varying Hb concentrations.

Clinical Neonatal Studies

Our neonatal studies confirmed the ability of our device to obtain signal measurements from the neonatal SSS in both reflection mode and transmission mode at the anterior and posterior fontanelles. The anterior fontanelle was the easiest to access due to larger size and anterior location. The posterior fontanelle was smaller in size and required repositioning of the neonates in order to access (posterior scalp location) which lead to more neonatal movement and difficulty in obtaining oxygen saturation measurements. We were able to provide stable continuous monitoring at the anterior and posterior fontanelles with real time display showing variability in measurements only when the neonates moved significantly during our exams. The fast signal acquisition available with our device allows for stable oxygen saturation measurements even with minimal neonatal head movements which is ideal for neonates and infants who cannot follow commands.

The average oxygen saturation measurement at the anterior fontanelle during ideal examination (sleeping with little movement) was 64.5% with a standard deviation of 1.8%. The average oxygen saturation measurement at the posterior fontanelle during ideal examination was 66.8% with a standard deviation of 1.3%. While the posterior fontanelles were patent during our examinations the skull bones adjacent to the posterior fontanelle can cover the opening immediately postpartum due to the pressure from passage through the vaginal canal and could limit its use in the immediate postpartum period.

The transmission mode was able to obtain oxygen saturation measurements but was technically much more difficult due to placement of two different devices (laser and acoustic probe). Future studies are needed to evaluate its feasibility as a tool for oxygen saturation measurements. Unfortunately the gold standard for confirming the accuracy of our SSS oxygen saturation measurements would be an invasive catheter obtaining venous samples from the SSS which is practically unattainable in neonates. Alternatively we could correlate measurements with invasive internal jugular venous samples, which is technically difficult and has multiple complications including infection and thrombosis and would be dangerous and unethical in a neonatal study.

The neonates we evaluated were medically stable at the time of measurements (i.e., no evidence of active hypoxia) with the measurements likely representing levels of a normal oxygenation state. Normal adult internal jugular vein oxygen saturation is abnormal under 50% or over 75% [26]. Our oxygen saturation measurements obtained at the anterior fontanelle (64.5%) and posterior fontanelle (66.8%) were well within the normal range for adults, as was expected due to the neonates being clinically stable. We did not find any levels below 50% which is considered abnormal for adults. The ability to monitor at-risk infants immediately postpartum may be difficult to due to medical care taking precedence. This highlights the advantage of having an easily maneuverable diagnostic tool that can safely and rapidly evaluate for cerebral hypoxia such as our laser diode based system. When there is a concern for peripartum cerebral hypoxia such as prolonged labor, abnormal

fetal heart tones, premature labor, eclampsia, premature rupture of membranes or placenta abruption amongst others, our system could be prepared prior to delivery to document cerebral oxygen saturation measurements within seconds after delivery without significantly impeding care.

Our study obtained neonatal cerebral venous oxygen saturation measurements in stable neonates typically hours to days after delivery. As such this initial study provides us a snapshot of neonatal cerebral oxygen saturation. The cerebral hemodynamics during labor and immediately post labor are complicated and have not been well established. As mentioned previously, several NIRS studies have shown that cerebral oxygenation appears to change in the normal postnatal time period [26]. Further studies are needed to evaluate what range of cerebral venous oxygen saturation measurements might be obtained immediately post-partum in neonates with risk factors for cerebral hypoxia (low birth weight, very low birth rate, early gestational age [14]) and those with normal labor to evaluate if an oxygen saturation difference between these groups can be identified. Measurements need to be monitored continuously to evaluate what normal changes might happen in this postnatal period. If a difference can be found between these two groups then a threshold for which cerebral venous oxygen saturation levels are concerning for hypoxia can be established with the ultimate goal of identifying which neonates have cerebral hypoxia and which could benefit from hypothermia treatment.

Caveats and Alternatives

An alternative to performing plastisol phantom studies with a NG:IL solution would have been to use fresh hemoglobin from an animal model, as was performed on previous studies [45,54,55]. Using animal hemoglobin would provide a better model when compared to NG:IL solution but has many technical difficulties such as keeping the blood uncoagulated, corporeal blood oxygenator and layering inhomogeneity over time. An

NG:IL solution was ultimately used due to ease of access, success with prior studies, and ultimately provided information to satisfy our goal which was to characterize the signal from a neonatal SSS phantom and how the signal amplitude varied at different depths and lateral displacement. We did not evaluate flow with our NG:IL solution which our group has done in prior studies with plastisol phantom and sheep models [45,53,55,59] as our main focus was on signal characterization rather than oxygen saturation measurements. Since the SSS drains the cerebral cortex our measurements could potentially not identify ischemia in structures drained by other veins such as the brainstem or cerebellum. This likely is not of concern as HIE or perinatal asphyxia is thought to occur from global hypoxia rather than a focal insult. Our device was able to successfully identify the neonatal SSS and obtain measurements in predominately term neonates. Very premature neonates may have much smaller SSS anatomy that could limit signal acquisition but fortunately our previous sheep studies were able to obtain measurements in an SSS measuring as small as 2-3 mm in width [55]. Finally our neonatal studies utilized only 15 neonates. More neonates will need to be recruited with analysis of differences between sex, gestational age and birth weight to identify any changes in venous oxygen saturation between these groups to establish what a normal range is within neonates.

Future Directions

As this was a preliminary study we wanted to initially evaluate if we could obtain signal from neonates and then what range could be found in stable neonates without signs of hypoxia. As neonatal cerebral hemodynamics are not well established, future studies can be performed in neonates within the immediate postpartum period and then at a later time to evaluate what cerebral venous oxygen saturation measurements can be obtained and if there is a normal physiologic change in the neonate during this early timeframe. This can then establish what normal range and changes can be expected. Additional studies could

also compare the laser optoacoustic measurements taken in neonates who already have an invasive catheter in place and compare with their actual venous oxygen saturation. While this is uncommon, some major centers which perform neonatal cardiovascular surgeries may have this ability. If these future studies demonstrate that our readings and direct samples give comparable measurements then we have established a device that can safely and quickly provide accurate cerebral venous oxygen saturation which clinicians can use in diagnosing cerebral hypoxia.

Chapter 7 CONLCUSION

Cerebral hypoxia can cause severe morbidity and mortality in neonates leading to increased health care costs globally and emotional toll on the family members involved with survivors that have lifelong disabilities. There is a crucial need for a safe, noninvasive and rapid method to screen neonates and stratify who would benefit from therapeutic hypothermia to further improve outcome. Our initial studies were able to demonstrate how our LDS optoacoustic system can obtain stable continuous monitoring of neonatal SSS venous oxygen saturation measurements in the reflection mode and transmission mode with an acoustic probe specifically designed for clinical use [78–80]. Further studies are needed to increase the number of neonates involved to find what normal neonatal cerebral venous oxygen saturation range are seen in the immediate postpartum timeframe with evaluation for differences in neonates with risk factors for cerebral hypoxia.

Bibliography/References

1. Vannucci SJ, Hagberg H. Hypoxia-ischemia in the immature brain. J Exp Biol. 2004;207(18):3149–54.

2. Johnston M V., Fatemi A, Wilson MA, Northington F. Treatment advances in neonatal neuroprotection and neurointensive care. Lancet Neurol. 2011;10(4):372–82.

3. Van Handel M, Swaab H, De Vries LS, Jongmans MJ. Long-term cognitive and behavioral consequences of neonatal encephalopathy following perinatal asphyxia: A review. Eur J Pediatr. 2007;166(7):645–54.

4. Kurinczuk JJ, White-Koning M, Badawi N. Epidemiology of neonatal encephalopathy and hypoxic-ischaemic encephalopathy. Early Hum Dev. 2010;86(6):329–38.

5. Douglas-Escobar M, Weiss MD. Hypoxic-ischemic encephalopathy: a review for the clinician. JAMA Pediatr. 2015;169(4):397–403.

6. Lawn JE, Cousens S, Zupan J. Neonatal Survival 1 4 million neonatal deaths : When ? Where ? Why ? Lancet. 2005;32(6):9–18.

7. Evans K, Rigby a S, Hamilton P, Titchiner N, Hall DM. The relationships between neonatal encephalopathy and cerebral palsy: a cohort study. J Obstet Gynaecol. 2001;21(2):114–20.

8. Pierrat V, Haouari N, Liska A, Thomas D, Subtil D, Truffert P. Prevalence, causes, and outcome at 2 years of age of newborn encephalopathy: population based study. Arch Dis Child Fetal Neonatal Ed. 2005;90(3):F257-61.

9. Gill MB, Perez-Polo JR. Hypoxia ischemia-mediated cell death in neonatal rat brain. Neurochem Res. 2008;33(12):2379–89.

10. Volpe JJ. Neonatal encephalopathy: An inadequate term for hypoxic-ischemic encephalopathy. Ann Neurol. 2012;72(2):156–66.

11. Hagberg H, Mallard C, Rousset Catherine CI, Wang X. Apoptotic mechanisms in the immature Brain: Involvement of mitochondria. J Child Neurol. 2009;24(9):1141–6.

12. Edwards, A. D., Yue, X., Squier, M.V., THoresen, M., Cady, E.B., Penrice, J., Cooper, C.E., Wyatt, J.S., Reynolds, E.O.R., Mehmet H. Specfici Inhibition of Apoptosis after Cerebral Hypoxia-Ischemia by Moderate Post-Insult Hypothermia. Biochem Biophys Reseach Commun. 1995;217(3):1193–9.

13. Jacobs SE, Berg M, Hunt R, Tarnow-Mordi WO, Inder TE, Davis PG. Cooling for newborns with hypoxic ischaemic encephalopathy. Cochrane Database Syst Rev. 2013;2013(1).

14. Nayeri F, Shariat M, Dalili H, Bani Adam L, Zareh Mehrjerdi F, Shakeri A. Perinatal risk factors for neonatal asphyxia in Vali-e-Asr hospital, Tehran-Iran. Iran J Reprod Med. 2012;10(2):137–40.

15. Shankaran S, Pappas A, McDonald SA, Vohr BR, Hintz SR, Yolton K, Gustafson KE, Leach TM, Green C, Bara R, Petrie Huitema CM, Ehrenkranz RA, Tyson JE, Das A, Hammond J, Peralta-Carcelen M, Evans PW, Heyne RJ, Wilson-Costello DE, Vaucher YE, Bauer CR, Dusick AM, Adams-Chapman I, Goldstein RF, Guillet R, Papile LA, Higgins RD. Childhood outcomes after hypothermia for neonatal encephalopathy. Obstet Gynecol Surv. 2012;67(10):617–9.

16. Azzopardi D V., Strohm B, Edwards AD, Dyet L, Halliday HL, Juszczak E, Kapellou O, Levene M, Marlow N, Porter E, Thoresen M, Whitelaw A, Brocklehurst P. Moderate Hypothermia to Treat Perinatal Asphyxial Encephalopathy. N Engl J Med. 2009;361(14):1349–58.

17. Alderson P, Gadkary C, Signorini DF. Therapeutic hypothermia for head injury. Cochrane Database Syst Rev. 2004;4(4):CD001048.

18. Thoresen M, Tooley J, Liu X, Jary S, Fleming P, Luyt K, Jain A, Cairns P, Harding D, Sabir H. Time is brain: Starting therapeutic hypothermia within three hours after birth improves motor outcome in asphyxiated newborns. Neonatology. 2013;104(3):228–33.

19. Guillet R, Edwards AD, Thoresen M, Ferriero DM, Gluckman PD, Whitelaw A, Gunn AJ. cooling for neonatal encephalopathy. 2012;71(2):205–9.

20. Andresen M, Gazmuri JT, Marín A, Regueira T, Rovegno M. Therapeutic hypothermia for acute brain injuries. Scand J Trauma Resusc Emerg Med. 2015;23:42.

21. Thoresen M, Penrice J, Lorek A, Cady EB, Wylezinska M, Kirkbride V, Cooper CE, Brown GC, Edwards AD, Wyatt JS, Reynolds EO. Mild hypothermia after severe transient hypoxia-ischemia ameliorates delayed cerebral energy failure in the newborn piglet. Pediatr Res. 1995;37(5):667–70.

22. Burton VJ, Gerner G, Cristofalo E, Chung S en, Jennings JM, Parkinson C, Koehler RC, Chavez-Valdez R, Johnston M V., Northington FJ, Lee JK. A pilot cohort study of cerebral autoregulation and 2-year neurodevelopmental outcomes in neonates with hypoxic-ischemic encephalopathy who received therapeutic hypothermia. BMC Neurol. 2015;15(1):209.

23. Macmillan CS, Andrews PJ. Cerebrovenous oxygen saturation monitoring: practical considerations and clinical relevance. Intensive Care Med. 2000;26(8):1028–36.

24. Gopinath SP, Valadka AB, Uzura M, Robertson CS. Comparison of jugular venous oxygen saturation and brain tissue Po2 as monitors of cerebral ischemia after head injury. Crit Care Med. 1999;27(11):2337–45.

25. Gopinath SP, Robertson CS, Contant CF, Hayes C, Feldman Z, Narayan RK, Grossman RG, Gopinath C S Robertson C F Contant C Hayes Z Feldman R K Narayan R G Grossman SP, Gopinath SP. Jugular venous desaturation and outcome after head injury. J ofNeurology, Neurosurgery, Psychiatry. 1994;57:717–23.

26. Dix LML, van Bel F, Lemmers PMA. Monitoring Cerebral Oxygenation in Neonates: An Update. Front Pediatr. 2017;5:46.

27. Peng S, Boudes E, Tan X, Saint-Martin C, Shevell M, Wintermark P. Does Near-Infrared Spectroscopy Identify Asphyxiated Newborns at Risk of Developing Brain Injury during Hypothermia Treatment? Am J Perinatol. 2015;32(6):555–64.

28. Schell RM, Cole DJ. Cerebral Monitoring: Jugular Venous Oximetry. Anesth Analg. 2000;90(3):559–66.

29. Rudinsky BF, Meadow WL. Internal Jugular Venous Oxygen Saturation Does Not Reflect Sagittal Sinus Oxygen Saturation in Piglets. Neonatology. 1991;59(5):322–8.

30. Hermansen MC, Hermansen GM. Intravascular catheter complications in the neonatal intensive care unit. Clin Perinatol. 2005;32(1):141–56.

31. Wiberg-Itzel E, Lipponer C, Norman M, Herbst A, Prebensen D, Hansson A, Bryngelsson AL, Christoffersson M, Sennström M, Wennerholm UB, Nordström L. Determination of pH or lactate in fetal scalp blood in management of intrapartum fetal distress: Randomised controlled multicentre trial. BMJ. 2008;336(7656):1284–7.

32. van Laerhoven H, de Haan TR, Offringa M, Post B, van der Lee JH. Prognostic tests in term neonates with hypoxic-ischemic encephalopathy: a systematic review. Pediatrics. 2013;131(1):88–98.

33. Glass HC, Glidden D, Jeremy RJ, Barkovich AJ, Ferriero DM, Miller SP. Clinical Neonatal Seizures are Independently Associated with Outcome in Infants at Risk for Hypoxic-Ischemic Brain Injury. J Pediatr. 2009;155(3):318–23.

34. Bogdanovic G, Babovic A, Rizvanovic M, Ljuca D, Grgic G, DjuranovicMilicic J. Cardiotocography in the Prognosis of Perinatal Outcome. Med Arch. 2014;68(2):102.

35. Chen H-Y, Chauhan SP, Ananth C V., Vintzileos AM, Abuhamad AZ. Electronic fetal heart rate monitoring and its relationship to neonatal and infant mortality in the United States. Am J Obstet Gynecol. 2011;204(6):491.e1-491.e10.

36. Alfirevic Z, Devane D, Gyte GML, Cuthbert A. Continuous cardiotocography (CTG) as a form of electronic fetal monitoring (EFM) for fetal assessment during labour. Cochrane Database Syst Rev. 2017;3(3).

37. Brazy JE. Cerebral oxygen monitoring with near infrared spectroscopy: Clinical application to neonates. J Clin Monit. 1991;7(4):325–34.

38. Tobias JD. Cerebral oxygenation monitoring: Near-infrared spectroscopy. Expert Rev Med Devices. 2006;3(2):235–43.

39. Kurth CD, Levy WJ, McCann J. Near-infrared spectroscopy cerebral oxygen saturation thresholds for hypoxia-ischemia in piglets. J Cereb Blood Flow Metab. 2002;22(3):335–41.

40. Tan ST. Cerebral oximetry in cardiac surgery. Hong Kong Med J. 2008;14(3):220–5.

41. Nebout S, Pirracchio R. Should we monitor ScVO2 in critically Ill patients? Cardiol Res Pract. 2012;2(1):1–7.

42. Sood BG, McLaughlin K, Cortez J. Near-infrared spectroscopy: Applications in neonates. Semin Fetal Neonatal Med. 2015;20(3):164–72.

43. Dix LML, van Bel F, Baerts W, Lemmers PMA. Comparing near-infrared spectroscopy devices and their sensors for monitoring regional cerebral oxygen saturation in the neonate. Pediatr Res. 2013;74(5):557–63.

44. Grant PE, Roche-Labarbe N, Surova A, Themelis G, Selb J, Warren EK, Krishnamoorthy KS, Boas D a, Franceschini MA. Increased cerebral blood volume and oxygen consumption in neonatal brain injury. J Cereb Blood Flow Metab. 2009;29(10):1704–13.

45. Esenaliev RO, Larina I V., Larin K V., Deyo DJ, Motamedi M, Prough DS. Optoacoustic technique for noninvasive monitoring of blood oxygenation: a feasibility study. Appl Opt 2002;41(22):4722.

46. Larin K V, Larina I V, Motamedi M, Esenaliev RO. Optoacoustic laser monitoring of cooling and freezing of tissues. Quantum Electron. 2002;32(11):953–8.

47. Laufer J, Elwell C, Delpy D, Beard P. In vitro measurements of absolute blood oxygen saturation using pulsed near-infrared photoacoustic spectroscopy: Accuracy and resolution. Phys Med Biol. 2005;50(18):4409–28.

48. Esenaliev RO. Optoacoustic monitoring of physiologic variables. Front Physiol. 2017;8:01030.

49. Meglinski I V., Matcher SJ. Quantitative assessment of skin layers absorption and skin reflectance spectra simulation in the visible and near-infrared spectral regions.

Physiol Meas. 2002;23(4):741–53.

50.   Petrova IY, Petrov YY, Prough DS, Esenaliev RO. Clinical tests of highly portable 2-lb. laser diode-based noninvasive optoacoustic hemoglobin monitor. Proc SPIE. 2009;7177:717705–1.

51.   Bakker A, Smith B, Ainslie P, Smith K. Near-infrared spectroscopy. Appl Asp Ultrason Humans. 2012;66–88.

52.   Petrov Y, Prough D, Deyo D, Petrova I, Motamedi M, Esenaliev R. In vivo noninvasive monitoring of cerebral blood with optoacoustic technique. Conf Proc IEEE Eng Med Biol Soc. 2004;3:2052–4.

53.   Brecht HP, Prough DS, Petrov YY, Patrikeev I, Petrova IY, Deyo DJ, Cicenaite I, Esenaliev RO. In vivo monitoring of blood oxygenation in large veins with a triple-wavelength optoacoustic system. Opt Express. 2007;15(24):16261–9.

54.   Petrov IY, Petrov Y, Prough DS, Cicenaite I, Deyo DJ, Esenaliev RO. Optoacoustic monitoring of cerebral venous blood oxygenation though intact scalp in large animals. Opt Express. 2012;20(4):4159–67.

55.   Petrova IY, Petrov YY, Esenaliev RO, Deyo DJ, Cicenaite I, Prough DS. Noninvasive monitoring of cerebral blood oxygenation in ovine superior sagittal sinus with novel multi-wavelength optoacoustic system. Opt Express. 2009;17(9):7285–94.

56.   Petrov IY, Petrov Y, Prough DS, Deyo DJ, Cicenaite I, Esenaliev RO. Optoacoustic monitoring of cerebral venous blood oxygenation through extracerebral blood. Biomed Opt Express. 2012;3(1):125.

57.   Prahl S. http://omlc.org/spectra/hemoglobin/

58.   Esenaliev RO. Optoacoustic diagnostic modality: from idea to clinical studies with highly compact laser diode-based systems. J Biomed Opt. 2017;22(9):091512.

59.   Petrov IY, Wynne KE, Petrov Y, Esenaliev RO, Richardson CJ, Prough DS. Noninvasive, optoacoustic monitoring of cerebral venous blood oxygenation in newborns. Photons Plus Ultrasound Imaging Sens. 2012;8223:82231M.

60.   Petrov, I. Y., Petrov, Y., Prough, D. S., Richardson, C. J., Fonseca, R. A., Robertson, C. S., Asokan C V., Agbor, A., Esenaliev RO. Transmission (forward) mode, transcranial, noninvasive optoacoustic measurements for brain monitoring, imaging, and sensing. Proc SPIE. 2016;9708:97084-1-197084–8.

61.   Petrov I. Y., Fonseca R.A., C.J. Richardson, Petrov Y. Y., Prough D. S., Petrov A., Wynne K. WS, Esenaliev R.O. Monitoring Cerebral Venous Blood Oxygenation in Neonates with a Medical-grade Optoacoustic System. Proc SPIE. 2015;9323:932302-1-932302–5.

62. Petrov Y, Petrov IY, Esenaliev RO. Nooninvasive Optoacoustic System for Rapid Diagnostics and Management of Circulatory Shock. Proc SPIE. 2013;8581:85814Y–85814Y7.

63. Petrov A, Wynne KE, Parsley MA, Petrov IY, Petrov Y, Ruppert KA, Prough DS, DeWitt DS, Esenaliev RO. Optoacoustic detection of intra- and extracranial hematomas in rats after blast injury. Photoacoustics. 2014;2(2):75–80.

64. Slovis TL, Kuhns LR. Real-time sonography of the brain through the anterior fontanelle. Am J Roentgenol. 1981;136(2):277–86.

65. Kiesler J, Ricer R. The abnormal fontanel. Am Fam Physician. 2003;67(12):2547–52.

66. Faix RG. Fontanelle size in black and white term newborn infants. J Pediatr. 1982;100(2):304–6.

67. Correa F, Enríquez G, Rosselló J, Lucaya J, Piqueras J, Aso C, Vázquez E, Ortega A, Gallart A. Posterior fontanelle sonography: An acoustic window into the neonatal brain. Am J Neuroradiol. 2004;25(7):1274–82.

68. Jacques SL. Optical properties of biological tissues: a review. Phys Med Biol. 2013;58(11):R37-61.

69. Spirou GM, Oraevsky AA, Vitkin IA, Whelan WM. Optical and acoustic properties at 1064 nm of polyvinyl chloride-plastisol for use as a tissue phantom in biomedical optoacoustics. Phys Med Biol. 2005;50(14):N141-53.

70. Simpson CR, Kohl M, Essenpreis M, Cope M. Near-infrared optical properties of ex vivo human skin and subcutaneous tissues measured using the Monte Carlo inversion technique. Phys Med Biol. 1998;43(9):2465–78.

71. Cheong W-F, Prahl SA, Welch AJ. A Review of the Optical Properties of Biological Tissues. IEEE J Quantum Electron. 1990;26(12):2166–85.

72. Patrikeev I, Petrov YY, Petrova IY, Prough DS, Esenaliev RO. Monte Carlo modeling of optoacoustic signals from human internal jugular veins. Appl Opt. 2007;46(21):4820–7.

73. Driver I, Feather JW, King PR, Dawson JB. The optical properties of aqueous suspensions of Intralipid, a fat emulsion. Phys Med Biol. 1989;34(12):1927.

74. Flock ST, Jacques SL, Wilson BC, Star WM, van Gemert MJC. Optical properties of intralipid: A phantom medium for light propagation studies. Lasers Surg Med. 1992;12(5):510–9.

75. van Staveren HJ, Moes CJ, van Marie J, Prahl S a, van Gemert MJ. Light scattering in Intralipid-10% in the wavelength range of 400-1100 nm. App Opt.

1991;30(31):4507–14.

76. Jacques SL. https://omlc.org/spectra/intralipid/.

77. Iizuka MN, Sherar MD, Vitkin IA. Optical phantom materials for near infrared laser photocoagulation studies. Lasers Surg Med. 1999;25(2):159–69.

78. Herrmann S, Petrov IY, Petrov Y, Richardson CJ, Fonseca RA, Prough DS, Esenaliev RO. Cerebral blood oxygenation measurements in neonates with optoacoustic technique. 2017;10064:100640Q.

79. Herrmann S, Petrov IY, Petrov Y, Fonseca A, Richardson CJ, Herrmann S, Petrov IY, Petrov Y, Fonseca RA, Richardson J, Shanina E, Prough DS, Esenaliev RO. Noninvasive measurement of cerebral venous oxygenation in neonates with a multi-wavelength, fiber-coupled laser diode optoacoustic system. Proc SPIE. 2018;1049409(March):1049409–6.

80. Herrmann S., Petrov I.Y., Petrov Y., Fonseca R.A., Richardson C.J., Shanina E., Prough D.S. ERO. Evaluation of neonatal cerebral venous oxygen saturation with laser diode optoacoustic system [abstract]. In: SPIE Medical Imaging: Ultrasonic Imaging and Tomography. 2018.

Vita

Stephen Alexander Herrmann 10/04/1984

Parents: Robert and Yolanda Herrmann

Texas Tech University- BA Psychology

Texas Tech Health Sciences Center- MS Molecular Pathology

University of Texas Houston- MD

University of Texas Houston Department of Internal Medicine- Internship

University of Texas Medical Branch Galveston- Radiology Residency PGY-5

Chief Resident- UTMB Radiology Residency Program

University of Texas Medical Branch Galveston- Dept. of Neuroscience,

Neurobiology of disease tract, PhD Candidate